Journal of Magnetic Resonance **152,** 132–148 (2001)
doi:10.1006/jmre.2001.2372, available online at http://www.idealibrary.com on IDEAL®

A New Approach to Visualizing Spectral Density Functions and Deriving Motional Correlation Time Distributions: Applications to an α-Helix-Forming Peptide and to a Well-Folded Protein

Djaudat Idiyatullin, Vladimir A. Daragan, and Kevin H. Mayo[1]

Department of Biochemistry, Molecular Biology, and Biophysics, University of Minnesota Health Science Center, 321 Church Street, Minneapolis, Minnesota 55455

E-mail: mayox001@tc.umn.edu

Received January 26, 2001; revised April 12, 2001; published online July 6, 2001

A new approach to visualizing spectral densities and analyzing NMR relaxation data has been developed. By plotting the spectral density function, $J(\omega)$, as $F(\omega) = 2\omega J(\omega)$ on the log–log scale, the distribution of motional correlation times can be easily visualized. $F(\omega)$ is calculated from experimental data using a multi-Lorentzian expansion that is insensitive to the number of Lorentzians used and allows contributions from overall tumbling and internal motions to be separated without explicitly determining values for correlation times and their weighting coefficients. To demonstrate the approach, ^{15}N and ^{13}C NMR relaxation data have been analyzed for backbone NH and $C_\alpha H$ groups in an α-helix-forming peptide 17mer and in a well-folded 138-residue protein, and the functions $F(\omega)$ have been calculated and deconvoluted for contributions from overall tumbling and internal motions. Overall tumbling correlation time distribution maxima yield essentially the same overall correlation times obtained using the Lipari–Szabo model and other standard NMR relaxation data analyses. Internal motional correlational times for NH and $C_\alpha H$ bond motions fall in the range from 100 ps to about 1 ns. Slower overall molecular tumbling leads to better separation of internal motional correlation time distributions from those of overall tumbling. The usefulness of the approach rests in its ability to visualize spectral densities and to define and separate frequency distributions for molecular motions.

Key Words: **peptides; NMR; ^{13}C and ^{15}N relaxation; spectral density; correlation time distributions.**

INTRODUCTION

One of the best ways to describe molecular motion is by using spectral density functions, $J(\omega)$, which present a distribution of frequencies for overall molecular tumbling and internal motions of a given vector, one that usually connects two interacting dipoles. Although spectral density functions can be calculated using optical and dielectric measurements, NMR relaxation provides the most reliable data for calculating $J(\omega)$. In NMR, the main relaxation parameters ($R_1 = 1/T_1$, $R_2 = 1/T_2$ and cross-relaxation rates calculated from NOE and T_1 data) are linear combinations of $J(\omega_i)$ at various frequencies. For ^{13}C NMR relaxation, equations for R_1, R_2, and NOE can be written as

$$R_1 = \frac{1}{10}k_{dd}[J(\omega_C - \omega_H) + 3J(\omega_C) + 6J(\omega_C + \omega_H)] + \frac{2}{15}\Delta\sigma^2\omega_C^2 J(\omega_C) \quad [1a]$$

$$R_2 = \frac{1}{20}k_{dd}[J(\omega_C - \omega_H) + 3J(\omega_C) + 6J(\omega_C + \omega_H) + 4J(0) + 6J(\omega_H)] + \frac{1}{45}\Delta\sigma^2\omega_C^2[4J(0) + 3J(\omega_C)] + R_{ex} \quad [1b]$$

$$\mathrm{NOE} = \frac{1}{10}\frac{\gamma_H}{\gamma_C}\frac{k_{dd}[6J(\omega_C + \omega_H) - J(\omega_C - \omega_H)]}{R_1}, \quad [1c]$$

where $k_{dd} = n\gamma_C^2\gamma_H^2\hbar^2/r_{CH}^6$, γ_C and γ_H are magnetogyric ratios for ^{13}C and ^{1}H nuclei, $\hbar$ is Plank's constant divided by 2π, r_{CH} is the length of the C–H bond, and n is the number of protons bonded to carbon. Equation [1c] is valid only for $n = 1$. For CH_2 and CH_3 groups, equations for the NOE are more complicated (*1, 2*).

As is evident in Eqs. [1], these relaxation parameters are described by five spectral densities, $J(0)$, $J(\omega_C)$, $J(\omega_H)$, $J(\omega_H - \omega_C)$, and $J(\omega_C + \omega_H)$ (for ^{13}C relaxation), as well as by a term to account for chemical exchange, R_{ex}. Because these six unknown terms cannot be determined using only three experimental parameters, i.e., R_1, R_2, and NOE, Peng and Wagner (*3, 4*) proposed using additional, more complicated relaxation experiments to be able to determine all five values of $J(\omega)$ at a given magnetic field. In their analysis, values for $J(\omega)$ that are evaluated at select frequencies are independent of any motional model or analytical form of the spectral density function. For this, six relaxation parameters are measured: T_1, T_2, NOE, longitudinal two-spin order, transverse relaxation rates of antiphase

[1] To whom correspondence should be addressed. Fax: 612-624-5121.

1090-7807/01 $35.00

coherence, and the proton spin–lattice relaxation rate. This approach is referred to as spectral density mapping. Lately, Peng and Wagner (*5*), Farrow *et al*. (*6*), and Lefevre *et al*. (*7*) have modified this original approach by considering various approximations for $J(\omega)$ at high frequency that allow the number of experimental parameters to be reduced. In fact, most investigators only determine three values of the spectral density function, $J(0)$, $J(\omega_{C(orN)})$, and $J(\omega_H)$, i.e., the probabilities of having molecular motions at very low ($\omega = 0$), intermediate ($\omega = \omega_C$), and high ($\omega = \omega_H$) frequencies. Even though this information is very useful, many features of internal and overall motions may be overlooked and it would be more informative to have a continuous spectral density function covering the frequency range from $\omega = 0$ to $\omega = \omega_C + \omega_H$.

The solution to this problem is not trivial. Obviously, obtaining an infinite number of discrete values for $J(\omega)$ is impossible. However, one can consider some approximations to describe $J(\omega)$ in this frequency range. The simplest one was first suggested by Lipari and Szabo *(8, 9)*, who used two Lorentzians, $\tau/(1 + \tau^2\omega^2)$, to describe $J(\omega)$:

$$J(\omega) = S^2\frac{\tau_o}{1 + (\omega\tau_o)^2} + (1 - S^2)\frac{\tau}{1 + (\omega\tau)^2}. \qquad [2]$$

S^2 is the squared order parameter, τ_o is the overall correlation time, and $\tau = \tau_o\tau_i/(\tau_o + \tau_i)$ where τ_i is the correlation time for internal bond rotations. Although this approach works well in many cases, particularly with well-structured proteins, Eq. [2] is, strictly speaking, only valid for very specific types of motion, the simplest being isotropic overall tumbling with one independent internal motion described, for example, rotational jumps between two states. If, on the other hand, rotational jumps occur between three nonequivalent states, then one needs at least three Lorentzians to define $J(\omega)$ (*2, 10*). More complicated motions like wobbling-in-a-cone require an infinite number of Lorentzians (*11, 12*).

Some attempts have been made to describe molecular motions in a more realistic fashion. The most popular way is to use a three-Lorentzian approximation where one considers two internal motional correlation times (*13*) as given by

$$J(\omega) = S^2\frac{\tau_o}{1 + (\omega\tau_o)^2} + \left(1 - S_f^2\right)\frac{\tau_{of}}{1 + (\omega\tau_{of})^2} + \left(S_f^2 - S^2\right)\frac{\tau_{os}}{1 + (\omega\tau_{os})^2}. \qquad [3]$$

$\tau_{of} = \tau_o\tau_f/(\tau_o + \tau_f)$ and $\tau_{os} = \tau_o\tau_s/(\tau_o + \tau_s)$. τ_s and τ_f are correlation times for slow and fast internal motions. The squared order parameter for fast internal motions, S_f^2, mathematically describes the fastest decay of the time correlation function. The terms for fast internal motions, τ_f and S_f, can be interpreted as fluctuations within potential wells, whereas internal motions described by τ_s define slower conformational jumps between various states.

The presence of anisotropic overall tumbling further complicates analysis. Even for the simplest model of axially symmetric overall tumbling with a single internal bond rotation, $J(\omega)$ is defined by 12 Lorentzians (*14*), and at least two order parameters are needed to describe internal motional restrictions. A more realistic picture of molecular motion is much more complicated because a distribution of molecular shapes and overall correlation times must be considered, not to mention the numerous types of internal motions. Proteins can display a very broad spectrum of internal motions ranging from the slowest motions of large structural units to the fastest fluctuations of small groups of atoms. Therefore, the problem of describing $J(\omega)$ as accurately as possible becomes extremely important.

The best way to describe $J(\omega)$ is by using a multi-Lorentzian expansion, which for any motional model is given by

$$J(\omega) = \sum_{i=0}^{N}\frac{c_i\tau_i}{1 + (\omega\tau_i)^2}, \qquad [4]$$

where c_i are weighting coefficients with $\sum_{i=0}^{N} c_i = 1$. Considered a model-free analysis of molecular motion, Eq. [4] can be obtained from general considerations of molecular motions (*15, 16*). Despite the complexity in interpreting the parameters c and τ (*8, 9*), Eq. [4] is very useful for describing molecular motions.

Using a sum of Lorentzians to describe $J(\omega)$ has an advantage over spectral density mapping (*5*). Because Eq. [4] is valid at any magnetic field, B_o, performing NMR relaxation experiments at different values of B_o allows a large number of c and τ parameters to be obtained. By using T_1, T_2, NOE data acquired at a single field, three theoretical parameters, c_o, τ_o, and R_{ex}, can be derived, while using data acquired at two fields, parameters for three Lorentzians, c_o, τ_o, c_1, τ_1, $c_2 = 1 - c_0 - c_1$, τ_2, and W_{ex}, can be obtained, and so on. Because the number of Lorentzians, N, can be very large, one would, in principle, want to determine as many experimental parameters as possible. However, the problem of using a minimization protocol to find reasonably accurate values for c and τ is complicated, and for most intents and purposes usually can only be done for two Lorentzians, i.e., the Lipari–Szabo approach. To illustrate this point, c_i and τ_i values calculated for two and three Lorentzians are plotted in Fig. 1. Darkened areas in these c–τ maps indicate regions of finding acceptable sets for c_i and τ_i using relaxation parameters, $P_i = T_1$, T_2, and NOE, at three magnetic fields (^{1}H Larmor frequencies, $\nu_H = 250$, 500, and 800 MHz). Standard errors in determining P_i are less than 3%. It is apparent that a clear separation of contributions from different Lorentzians can only be obtained for two Lorentzians. Using three or more Lorentzians and experimental data having an average error greater than 3% yields no unique solution; i.e., accurate values for c and τ cannot be obtained. If anything, only the largest correlation times can be estimated within reasonable error. Moreover, there is a problem of interpretation. Even considering only two Lorentzians, τ_1 cannot simply

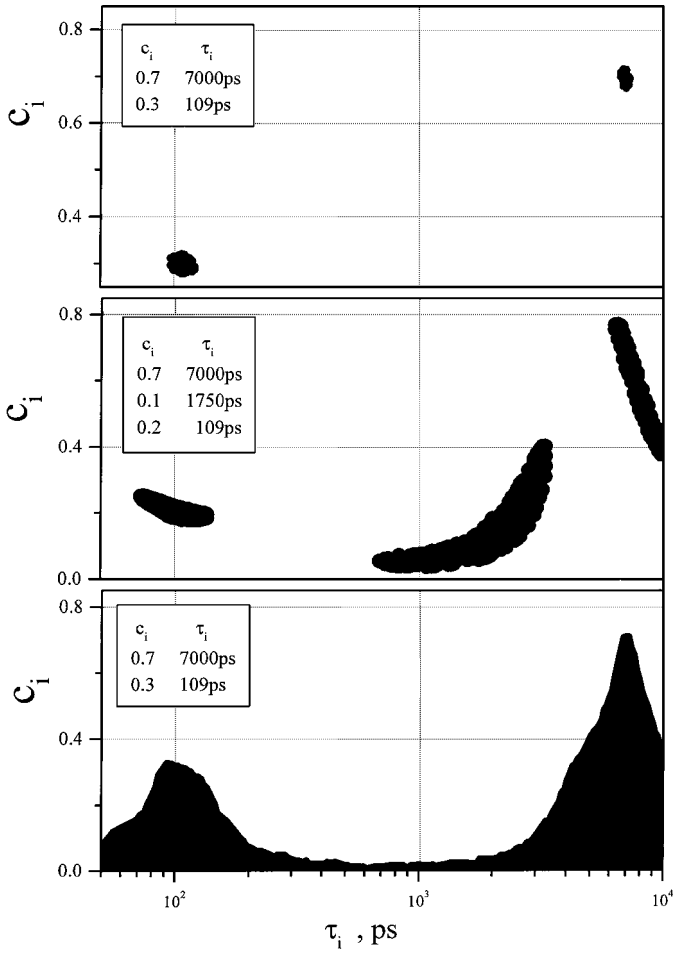

FIG. 1. A weighting coefficient–correlation time (c–τ) map calculated using Eq. [4] with two (top and bottom panels) or three (middle panel) Lorentzians. Dark areas give the probability of finding values for c and τ that can account for the relaxation parameters T_1, T_2, and NOE acquired at three magnetic fields (^{1}H frequencies, ν_H, of 250, 500, and 800 MHz). c and τ values within the dark areas correspond to standard deviations of experimental parameters that are less than 3% of parameters calculated for the given sets of c and τ shown in the figure.

be interpreted as the correlation time for internal motion because it is a mixture of correlation times for overall tumbling and internal motion (*8*, *9*), and in a system with two internal motional correlation times, τ_s and τ_f, one needs to consider combinations of correlation times, $1/\tau_o + 1/\tau_s$ and $1/\tau_o + 1/\tau_s + 1/\tau_f$ (*13*, *17*), in addition to the correlation time for overall tumbling. A similar problem arises when attempting to interpret values for c_i. Only in the simplest case, i.e., isotropic overall tumbling, can the coefficient c_0 be interpreted as the order parameter. All other coefficients are complicated combinations of various order parameters. For overall tumbling of an anisotropic molecule, even c_0 cannot be considered an order parameter. Another problem of using a multi-Lorentzian approximation to derive values for τ_i and c_i lies in choosing the correct number of Lorentzians that satisfactorily describe the motions of a given molecule. The bottom panel of Fig. 1 illustrates the case when one tries to determine parameters for three Lorentzians from the two-Lorentzian curve. The resulting broad distributions demonstrate the fact that choosing an incorrect number of Lorentzians can lead to substantial errors in determining values for c and τ.

For these reasons outlined above, an alternative approach is required. The present paper presents a novel approach that describes molecular motions as a distribution of correlation times. This method is not limited by the number of Lorentzians and avoids an explicit determination of values for c_i and τ_i.

METHODS AND MATERIALS

Peptide and protein production. Peptides having the amino acid sequence GFSKAELAKARAAKRGGY were synthesized using standard Fmoc solid-phase methodology (*18*) and were purified by HPLC using a linear acetonitrile/water gradient as described by Idiyatullin *et al*. (*19*). Five such peptides were made, each incorporating a single, ^{13}C/^{15}N-enriched amino acid (CIL, Cambridge). The residues enriched were F2, A5, L7, A8, and A10. Peptide purity was checked by MALDI-TOF mass spectrometry and analytical HPLC on a C18 Bondclone (Phenomenex) column. The 138-residue protein MMOB (methane monooxygenase component B) was produced as a recombinant protein as described by Chang *et al*. (*20*). For this, *E. coli* containing the expression system were grown on M9 minimal media containing ^{15}N-ammonium or ^{13}C-glucose, and MMOB was uniformly isotopically enriched in either ^{15}N or ^{13}C. For some ^{13}C relaxation experiments on MMOB, enrichment in ^{13}C was only to 40%.

NMR. For NMR measurements, freeze-dried samples were dissolved in D_2O for ^{13}C relaxation measurements or in a H_2O/D_2O (90/10) mixture for ^{15}N relaxation measurements. Peptide concentration, determined from the dry weight of freeze-dried samples, was 15 mg/mL. The pH was adjusted to pH 6 by adding microliter quantities of NaOD or DCl. NMR relaxation experiments were performed on Varian Inova-500, 600, 800 NMR spectrometers equipped with triple-resonance probes and on a Bruker AM-250 NMR spectrometer. The temperature was varied from 5 to 30°C. Temperature calibration was performed by using chemical shifts of resonances from methanol. Under these experimental conditions, pulse field gradient (PFG) self-diffusion measurements indicated that aggregation was not occurring (*19*).

Relaxation measurements on the peptide. ^{13}C spin–lattice relaxation rates with the peptide 17mer were determined by using the direct homonuclear inversion-recovery method with a composite 180° pulse (90°_x–180°_y–90°_x). In all experiments, broadband ^{1}H decoupling GARP (*21*) was used. The number of acquisitions was chosen to have a signal-to-noise ratio greater than 70. Therefore, the number of transients varied from 200 to 1000. Ten to 15 time incremented (partially

relaxed) spectra were routinely acquired for each relaxation measurement. ^{13}C spin–spin relaxation rates were measured by using the proton-detected HSQC pulse sequence as described below for the ^{15}N Carr–Purcell–Maiboom–Gill (CPMG) experiment (*22*) with some modification. Since each ^{13}C nucleus in this peptide has at least one ^{13}C-bonded carbon, J-coupling induces oscillations between in- and anti-phase coherence that modulates the spin-echo decay (*23*) and thus precludes measuring T_2 relaxation times with the CPMG pulse sequence. To eliminate effects from J-coupling, soft rectangular pulses at the ^{13}C resonance of interest were used. The duration, d, of the 180° pulse was 0.4 to 0.7 ms, and the time delay, t, in the CPMG pulse train was 0.9 ms. During the relaxation time, ^{15}N and ^{1}H broadband WALTZ-16 decoupling (*24*) was used. For $^{13}C_\alpha$ relaxation, soft ^{13}C pulses applied at the resonance of interest are selective; therefore, with each 180° pulse, the sign of the anti-phase coherence changes and the contribution is eliminated. The smoothness in the T_2 relaxation decay curves indicates that effects from J-coupling have been eliminated. Using this method, T_2 values are in good agreement with T_2 values measured by using the spin-locking experiment with small RF fields. This approach to measuring T_2 relaxation curves that are devoid of J-coupling effects, is, in effect, a combination of CPMG and spin-lock experiments. Relaxation rates were determined by using methods described by Daragan *et al.* (*25*), and ^{13}C–{^{1}H} NOE coefficients were measured by using the standard gated-decoupling technique.

^{15}N spin–lattice and spin–spin relaxation rates were measured by using the HSQC sequence reported by Farrow *et al*. (*22*). This pulse sequence employs pulsed field gradients for the coherence transfer pathway whereby magnetization passes from ^{1}H to ^{15}N and back again to ^{1}H for observation. The water flip-back method was used to minimize water saturation during the pulse sequence. During the relaxation time, ^{13}C broadband decoupling ($^{13}C_\alpha$H region) WALTZ-16 (*24*) was used. The delay in the CPMG train was 0.9 ms. Spin–lattice and spin–spin relaxation decays for all residues follow single exponential decays, except for F2, which shows two distinguishable exponents. After carrying out additional experiments with different concentrations of D_2O in H_2O, it was determined that the initial fast decay is related to proton detection and proton–deuterium exchange. Therefore, to more accurately determine relaxation parameters for F2, the slower decaying component was used. Steady-state {^{1}H}–^{15}N NOEs were determined from spectra recorded in the presence and absence of proton saturation (*23*). Saturation was achieved by application of 120° ^{1}H pulses every 5 ms (*26*) during repetition times of 5 s. When proton saturation was absent, a net relaxation delay of 10 s was used. Five pairs of these spectra were recorded in the same way and data reported here are the average of these five pairs of spectra.

Relaxation measurements on the protein. For the protein MMOB, 2D NMR versions of relaxation experiments were used, essentially as described above for the peptide. ^{15}NH T_1, T_2, and {^{1}H}–^{15}N NOEs were measured by using the standard inversion recovery, Carr–Purcell–Meiboom–Gill (CPMG) and steady-state NOE pulse sequences, respectively (*22*). Relaxation delays for ^{15}NH T_1 and T_2 were placed before the evolution period, and double INEPT pulse sequences were used to increase sensitivity, and a reverse INEPT sequence was employed to enhance steady-state NOEs. In all cases, gradient sensitivity-enhanced pulse sequences were used. Repetitive ^{1}H 180° pulses were applied during relaxation delays to suppress cross-correlation between dipolar and CSA relaxation, and a 1.25-ms delay was given between 180° pulses in the CPMG pulse sequence. For NOE measurements, a 3-s recycle delay was used, followed by 3 s of ^{1}H saturation. For $^{13}C_\alpha$H T_1 and NOE studies, the same relaxation experiments were used. For $^{13}C_\alpha$H T_2 measurements, however, off-resonance rotating frame $T_{1\rho}$ relaxation experiments were performed using pulse sequences described by Zinn-Justin *et al.* (*27*) and by Mulder *et al.* (*28*). $1/T_{1\rho} = R_{1\rho}$ can be expressed as $R_{1\rho} = R_1 \cos^2\theta + R_2 \sin^2\theta$, where θ is the angle between the effective spin-lock field and the B_0 field. To further reduce effects from ^{13}C–^{13}C scalar coupling and dipolar coupling between adjacent carbons in uniformly labelled ^{13}C-enriched proteins (*29*), MMOB was ^{13}C-enriched to only 40%.

Analysis of relaxation data. Motional parameters were determined by using a Monte Carlo minimization protocol (*25*). The function to be minimized is

$$\chi^2 = \sum_i \left[\left(R^i_{1\text{exp}} - R^i_{1\text{theor}}\right)/\sigma_{\text{R1}}\right]^2 + \left[\left(R^i_{2\text{exp}} - R^i_{2\text{theor}}\right)/\sigma_{\text{R2}}\right]^2 + \left[\left(\text{NOE}^i_{\text{exp}} - \text{NOE}^i_{\text{theor}}\right)/\sigma_{\text{NOE}}\right]^2, \quad [5]$$

where $R^i_{1\text{exp}}$, $R^i_{2\text{exp}}$, $\text{NOE}^i_{\text{exp}}$ are experimental values and $R^i_{1\text{theor}}$, $R^i_{2\text{theor}}$, $\text{NOE}^i_{\text{theor}}$ are calculated values of NMR relaxation parameters and expressed as spectral densities of molecular motions as defined by equations presented in the Introduction. The terms σ_{R1}, σ_{R2}, and σ_{NOE} are the standard errors of the experimental parameters. During minimization, the contribution due to chemical exchange, R_{ex}, was taken as being proportional to the Larmor frequency squared because Nesmelova *et al.* (*30*) demonstrated that the helix-forming peptide is at the fast-exchange limit. The summation in Eq. [5] was performed over all NMR frequencies for which data were acquired.

In addition, dipolar coupling between adjacent carbons in uniformly ^{13}C-labeled amino acids can contribute to carbon relaxation rates. In general, the effect is greater for molecules exhibiting larger overall tumbling correlation times and at higher magnetic fields. Because of this, relaxation data were corrected by assuming that contributions from C–H and C–C spectral densities were equal. This reasonable assumption contributed less than 2% to the error in calculating relaxation rates.

RESULTS AND DISCUSSION

Visualizing Spectral Density Functions

Figure 2A illustrates the standard graphical representation of a spectral density function, $J(\omega)$, consisting of two Lorentzians with $c_0 = 0.7$, $\tau_0 = 8000$ ps, $c_1 = 0.3$, and $\tau_1 = 100$ ps. These are realistic motional parameters for a globular protein in water and having a molecular weight of about 15,000 or for a peptide in water/TFE (higher viscosity) having a molecular weight of about 4,000. From this plot of $J(\omega)$ it is difficult or impossible to garner any meaningful information on molecular motion. However, when plotted on a log scale, this same spectral density function shows two inflections or "steps" (Fig. 2B) that may be used to estimate correlation times by taking their positions on the X axis as $\omega_i = 1/\tau_i$. To better visualize this, consider the function $F(\omega) = 2\omega J(\omega)$ as plotted in Fig. 2C. This way of visualizing $J(\omega)$ forms the basis of this new approach that aims to derive more meaningful information on molecular motions. $F(\omega)$ has some interesting properties. For instance, when motional correlation times are significantly different, $F(\omega)$ consists of fairly resolved, broad bands or peaks that are symmetric with their frequency maxima, ω_i, corresponding to the inverse of their correlation times, i.e., $\omega_i \approx 1/\tau_i$, and the position of their maxima on the Yaxis corresponding to coefficients c_i given in Eq. [4]:

$$\omega_{\max i} \approx 1/\tau_i \quad [6a]$$

$$F(\omega_{\max i}) \approx c_i. \quad [6b]$$

As the difference in correlation times becomes larger, Eqs. [6a] and [6b] become more exact. To prove this, consider a single Lorentzian, $F(\omega) = 2\omega\tau/(1 + \omega^2\tau^2)$ as shown in Fig. 3A. The first derivative of this function is zero when $\omega_{\max} = 1/\tau$ and $F(\omega_{\max}) = 1$. The linewidth of the peak can be defined in terms of the ratios

$$\omega_R/\omega_{\max} = \omega_{\max}/\omega_L, \quad [7]$$

where

$$F(\omega_R) = 0.5F(\omega_{\max}) \quad \omega_R > \omega_{\max}$$

$$F(\omega_L) = 0.5F(\omega_{\max}) \quad \omega_L < \omega_{\max}.$$

For a single Lorentzian, ratios in Eq. [7] do not depend on the correlation time, τ, and the ratio $\omega_{\max}/\omega_L$ equals $\omega_R/\omega_{\max}$ with both being equal to $2 + \sqrt{3} = 3.73$. These ratios are likewise equal to $(2 - \sqrt{3})^{-1} = 3.73$. The high- and low-frequency tails of $F(\omega) = 2c\omega\tau/(1 + \omega^2\tau^2)$ are given by

$$F(\omega) \to 2c\omega\tau \quad \text{as } \omega \to 0 \quad [8a]$$

$$F(\omega) \to 2c/\omega\tau \quad \text{as } \omega \to \infty. \quad [8b]$$

These limits are described by linear equations

$$\text{Log}(F(\omega)) = \text{Log}(2c\tau) + \text{Log}(\omega) \quad \text{for } \omega \to 0 \quad [9a]$$

$$\text{Log}(F(\omega)) = \text{Log}(2c/\tau) - \text{Log}(\omega) \quad \text{for } \omega \to \infty, \quad [9b]$$

such that the high- and low-frequency sides of the single Lorentzian function $F(\omega)$ are straight lines with slopes of $+45^\circ$ and -45°, respectively. These lines intersect at $\omega = 1/\tau$ to give a value of $2c$ read from the Y axis (see Fig. 3A).

With two well-defined and equally weighted Lorentzians, a log–log plot of $F(\omega)$ yields two peaks approximately positioned at $\omega_1 = 1/\tau_1$ and $\omega_2 = 1/\tau_2$ with the heights of the peaks being approximately equal to c_1 and c_2. The peak at lower frequency corresponds to the larger correlation time. Peak resolution depends on the values of τ_1 and τ_2 and the weighting coefficients c_1 and c_2. Individual peaks become resolved at a ratio $\tau_1/\tau_2 \approx 6$, and optimal resolution is obtained when $c_1 = c_2$. In this case, the spectrum is symmetric relative to ω_0,

$$\omega_0 = \frac{1}{\sqrt{\tau_1\tau_2}}, \quad [10]$$

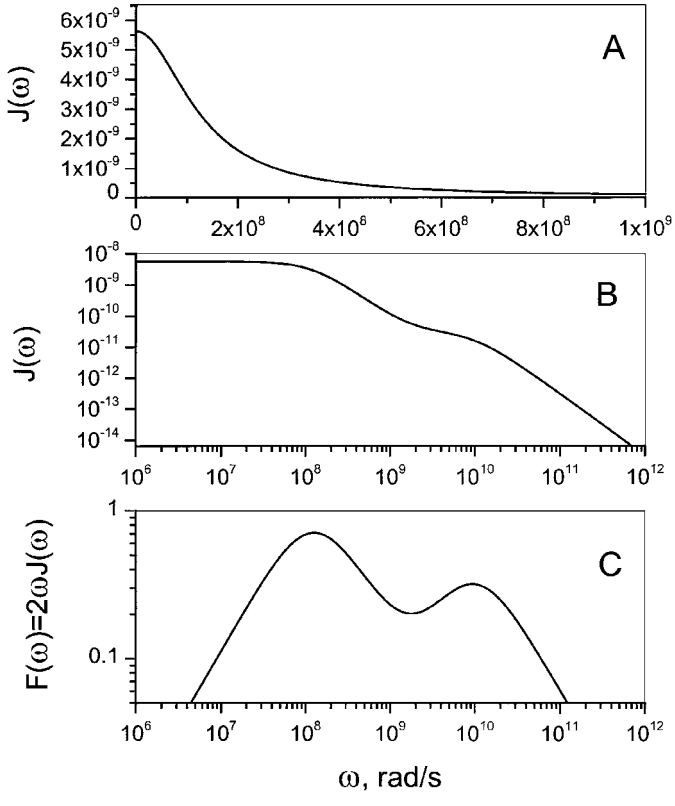

FIG. 2. Various presentations of the spectral density function $J(\omega)$. (A) $J(\omega)$ calculated using two Lorentzians with $\tau_0 = 8000$ ps, $\tau_1 = 100$ ps, $c_0 = 0.7$, $c_1 = 0.3$. (B) The same $J(\omega)$ plotted on the log scale. (C) The same $J(\omega)$ plotted as the function $F(\omega) = 2\omega J(\omega)$. In (C), two well-separated peaks positioned at $\omega_0 = 1/\tau_0$ and $\omega_1 = 1/\tau_1$ are observed and their amplitudes are approximately equal to the weighting coefficients c_0 and c_1.

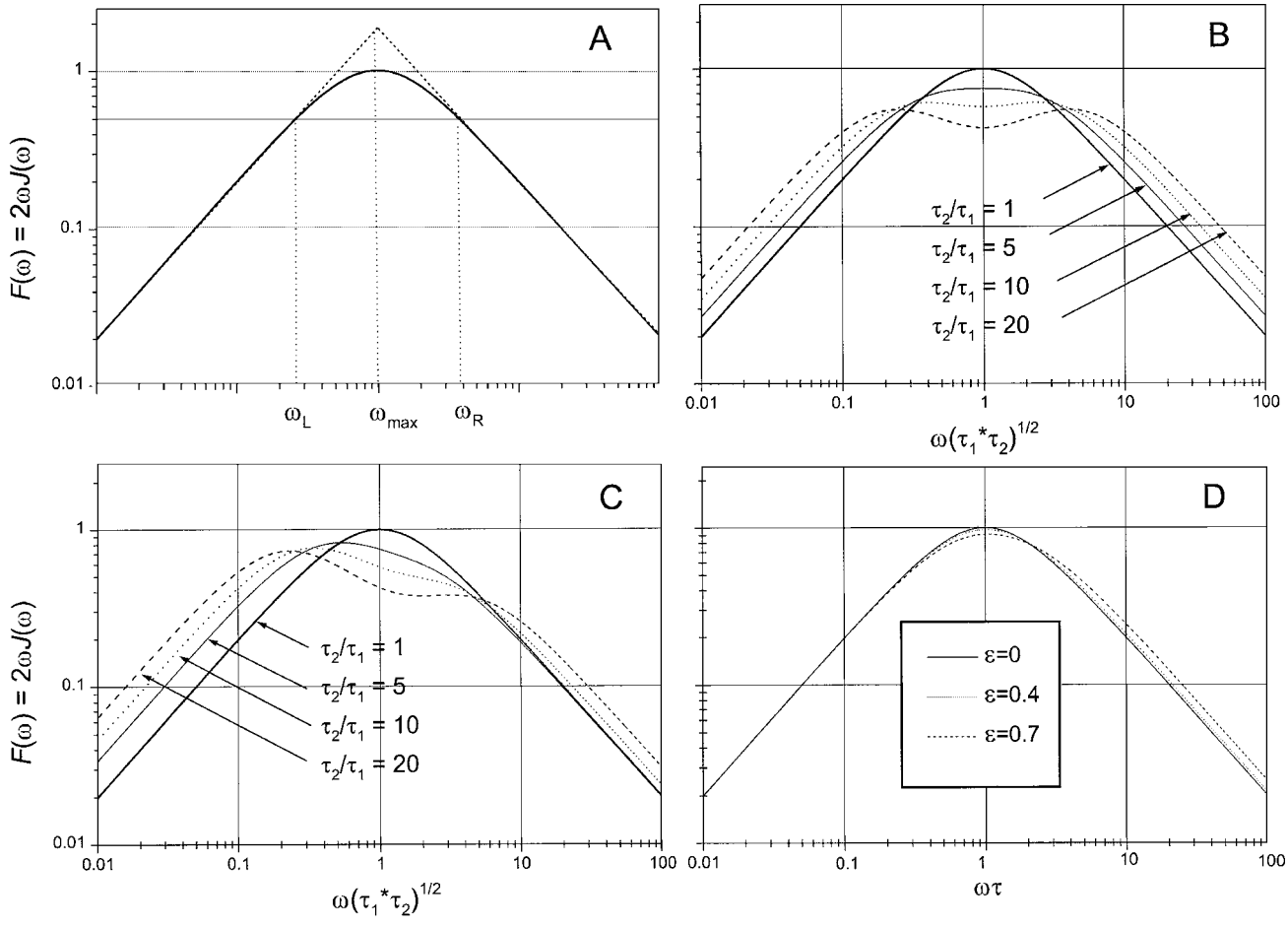

FIG. 3. Spectral density functions plotted as $F(\omega) = 2\omega J(\omega)$. (A) $F(\omega)$ calculated using a single Lorentzian. (B) $F(\omega)$ calculated using two Lorentzians and various values for τ_1 and τ_2 with $c_1 = c_2 = 0.5$. (C) $F(\omega)$ calculated using two Lorentzians and various values for τ_1 and τ_2 with $c_1 = 0.7$ and $c_2 = 0.3$. (D) $F(\omega)$ calculated using a rectangular distribution of correlation times as described in the text.

which is the position of the maximum when $F(\omega, \tau_1)$ and $F(\omega, \tau_2)$ are not resolved or the position of the central minimum when they are resolved. For $F(\omega) = F(\omega, \tau_1) + F(\omega, \tau_2)$, $F(\omega)$ is defined as

$$F(\omega_0) = \frac{2\sqrt{\tau_1\tau_2}}{\tau_1 + \tau_2}, \qquad [11]$$

when $c_1 = c_2 = 1/2$ and $\omega = \omega_0$. The high- and low-frequency maxima (if any) are positioned at ω_1 and ω_2:

$$\omega_{1,2} = \frac{|\tau_1 - \tau_2| \pm \sqrt{(\tau_1 - \tau_2)^2 - 4\tau_1\tau_2}}{2\tau_1\tau_2}. \qquad [12]$$

For the peaks to be resolved, τ_1 should be greater than τ_2 according to the condition

$$\tau_1/\tau_2 > 3 + 2\sqrt{2} \approx 5.8. \qquad [13]$$

When inequality [13] is true, two maxima are observed. Figure 3B plots $F(\omega) = F(\omega, \tau_1) + F(\omega, \tau_2)$ for different values of the ratio τ_2/τ_1 when $c_1 = c_2 = 0.5$. The lines remain symmetric, but become broader as the ratio of correlation times is increased.

When c_1 and c_2 are not equal, equations for the maximum positions become more complicated. Figure 3C plots $F(\omega) = F(\omega, \tau_1) + F(\omega, \tau_2)$ for $c_1 = 0.7$ and $c_2 = 0.3$ at different values of the ratio of correlation times. As τ_2/τ_1 increases from unity, $F(\omega)$ becomes more asymmetric, and on approaching $\tau_2/\tau_1 = 20$, component peaks become apparent. When analyzing actual experimental data, it is important to remember that the low-frequency side of $F(\omega)$ provides information on the contribution from overall molecular tumbling motions, whereas the higher frequency side of $F(\omega)$ contains contributions from both overall tumbling and internal motions.

In reality, a few discrete correlation times may not be sufficient to account for the relaxation data. This situation may exist, for example, with macromolecules where overall correlation times may, in fact, be some distribution due to various factors, e.g., slow conformational fluctuations, aggregation, and

complex formation. To exemplify this, consider the simplest case of a rectangular distribution with limits from τ_1 to τ_2 (and $\tau_2 > \tau_1$). With $\tau = (\tau_1 + \tau_2)/2$, $F(\omega)$ for this distribution can be expressed as

$$F(\omega, \varepsilon) = \frac{1}{\tau_2 - \tau_1} \int_{\tau_1}^{\tau_2} \frac{2\omega\tau}{1 + \omega^2\tau^2}\, d\tau$$

$$= \frac{1}{2\omega\tau\varepsilon} \ln\left(\frac{1 + \omega^2\tau^2(1+\varepsilon)^2}{1 + \omega^2\tau^2(1-\varepsilon)^2}\right), \qquad [14]$$

where

$$\varepsilon = (\tau_2 - \tau_1)/2\tau \qquad [15]$$

is the width of the correlation time distribution at half-height [$F(\omega, \varepsilon) = 0.5$] relative to its average correlation time, τ. Figure 3D plots $F(\omega, \varepsilon)$ for different values of ε. Note that at small values of ε, $F(\omega, \varepsilon)$ does not differ significantly from the single Lorentzian function, $F(\omega)$, and when ε becomes large, $F(\omega, \varepsilon)$ becomes asymmetric with its maximum being shifted to lower frequency. This asymmetry can be used, therefore, to find the presence of a distribution of correlation times.

One of the most significant problems in determining $J(\omega)$ using NMR relaxation data arises when trying to derive the parameters c_i and τ_i with a set number of Lorentzians that is insufficient to describe the spectral density function (*31*). This has been exemplified in Fig. 1C. Using the new approach with $F(\omega) = 2\omega J(\omega)$ circumvents this problem because $F(\omega)$ and the error in minimization do not depend on the number of Lorentzians used. Figure 4 shows the standard deviation, χ^2, of the calculated curve from the theoretical curve as a function of the number of Lorentzians, N, used in the minimization protocol. The theoretical function, $F(\omega)$, was created using 6 Lorentzians with $\tau_0 = 8000$ ps, $c_0 = 0.3$, $\tau_1 = 7000$ ps, $c_1 = 0.3$, $\tau_2 = 1500$ ps, $c_2 = 0.2$, $\tau_3 = 500$ ps, $c_3 = 0.1$, $\tau_4 = 100$ ps, $c_4 = 0.05$, $\tau_5 = 20$ ps, $c_5 = 0.05$, and the chemical exchange term R_{ex} set at 2 s^{-1} (at ^{1}H frequency of 800 MHz). These parameters are representative of some motional vector within a protein of molecular weight about 15,000. For this calculation, it was assumed that T_1, T_2, NOE data were measured at three spectrometer frequencies ($\nu_H = 250$, 500, and 800 MHz). Theoretically, only four Lorentzians can be used to fit nine experimental parameters. However, with the new approach, this limitation of using a larger number of Lorentzians (up to 8 as shown in Fig. 4) is avoided. In fact, data can be better fitted using a larger number of Lorentzians. Nevertheless, determination of a number of c_i and τ_i values that is larger than the number of experimental parameters cannot be done. This approach only allows the function $F(\omega)$ to be determined. Figure 4 also plots minimization-derived values for R_{ex} vs N and shows that using this approach, R_{ex} can be determined accurately with $N = 3$ or higher.

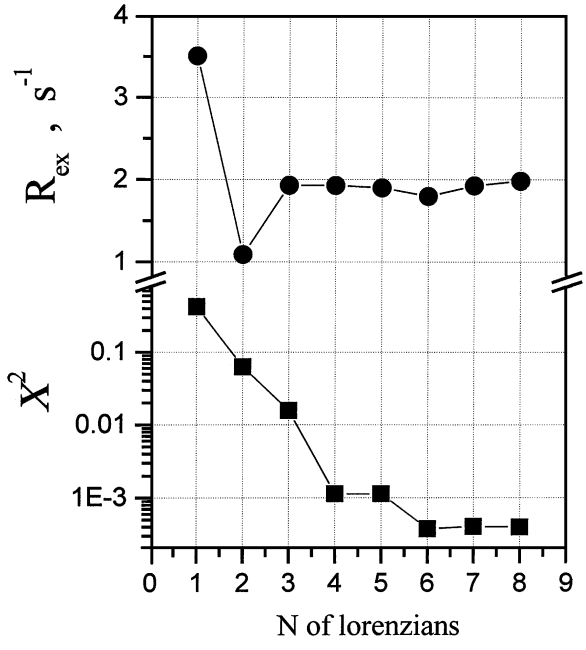

FIG. 4. The χ^2 error in fitting $F(\omega)$ as a function of number of Lorentzians used in the minimization procedure. Here, $F(\omega)$ is described by 6 Lorentzians with $\tau_0 = 8000$ ps, $c_0 = 0.3$, $\tau_1 = 7000$ ps, $c_1 = 0.3$, $\tau_2 = 1500$ ps, $c_2 = 0.2$, $\tau_3 = 500$ ps, $c_3 = 0.1$, $\tau_4 = 100$ ps, $c_4 = 0.05$, $\tau_5 = 20$ ps, $c_5 = 0.05$. The minimization procedure was performed using T_1, T_2, and NOE values acquired at three magnetic fields (^{1}H frequencies, ν_H, of 250, 500, and 800 MHz). At the top of the figure, the exchange terms, R_{ex}, at 800 MHz (^{1}H frequency) that result from minimization are also plotted vs the number of Lorentzians used.

Separating Overall Tumbling from Internal Motions

In this section, an approach that can be used to deconvolute $F(\omega)$ into components for overall tumbling, $F_o(\omega)$, and internal motions, $F_i(\omega)$, is reported. In general, $F(\omega)$ can be expressed as

$$F(\omega) = F_o(\omega) + F_i(\omega). \qquad [16]$$

From Eq. [4], an important property of $F(\omega)$ at low frequency is evident

$$\mathrm{Log}(F(\omega)) = \mathrm{Log}(2J(0)) + \mathrm{Log}(\omega) \quad \text{as } \tau_0\omega \to 0, \qquad [17]$$

where

$$J(0) = \sum c_i \tau_i \qquad [18]$$

is defined as the average correlation time. $J(0)$, which is approximately equal to $c_0\tau_0$, can be determined using Eq. [17], and an estimate of τ_0 can be derived from the low-frequency maximum, $F(\omega_{max})$, which is usually primarily the result of overall tumbling motions. For the two correlation time model with $\tau_1 \ll \tau_0$,

approximate equations can be obtained for

$$\omega_{\max} \approx \frac{1}{\tau_0}\left(1 + \frac{2c_1\tau_1}{c_0\tau_0}\right) \quad [19a]$$

and

$$F(\omega_{\max}) \approx c_0\left(1 + \frac{2c_1\tau_1}{c_0\tau_0}\right). \quad [19b]$$

Using these equations, τ_0 and c_0 can be determined with reasonable accuracy from the position of the maximum, $\omega_{\max}$, and the value of $F(\omega_{\max})$, and these values can, in turn, be used as initial approximations to separate $F_0(\omega)$ and $F_i(\omega)$ from $F(\omega)$. To achieve this deconvolution, a simple algorithm can be used:

1. Define $\tau_0 = 1/\omega_{\max};\ c_0 = F(\omega_{\max})$
2. Estimate $F_i(\omega)$ as $F_i(\omega) = F(\omega) - 2\omega\tau_0 c_0/(1+\omega^2\tau_0^2)$ (the low-frequency region is approximated by a single Lorentzian)
3. Find the maximum of $F_i(\omega)$, and set $\tau_1 = \omega_{\max}$ and $c_1 = F_i(\omega_{\max})$
4. Redefine $F_o(\omega)$ as $F_o(\omega) = F(\omega) - 2\omega\tau_1 c_1/(1+\omega^2\tau_1^2)$ (the high-frequency region $F_i(\omega)$ is approximated by a single Lorentzian)
5. Define $\tau_0 = 1/\omega_{\max}; c_0 = F_o(\omega_{\max})$
6. Repeat steps 2–5.

Usually, three to five iterations are sufficient to obtain $F_i(\omega)$ accurately. Figure 5A shows the use of this algorithm to calculate $F_i(\omega)$ with 5 Lorentzians and a single correlation time for overall tumbling. For this calculation, c and τ were taken as $c_0 = 0.7$, $\tau_0 = 8000$ ps; $c_1 = 0.1$, $\tau_1 = 1000$ ps; $c_2 = 0.1$, $\tau_2 = 700$ ps; $c_3 = 0.05$, $\tau_3 = 200$ ps, $c_4 = 0.05$, $\tau_4 = 20$ ps. The dotted line represents $F_i(\omega)$ calculated using these c and τ values, and the dashed line represents $F_i(\omega)$ determined by minimization using the algorithm given above. Figure 5B shows the results of minimization using a distribution of overall tumbling correlation times.The corresponding parameters for c and τ for this calculation were $c_0 = 0.2$, $\tau_0 = 8000$ ps; $c_1 = 0.2$, $\tau_1 = 7000$ ps; $c_2 = 0.2$, $\tau_2 = 6000$ ps; $c_3 = 0.2$, $\tau_3 = 1000$ ps; $c_4 = 0.1$, $\tau_4 = 200$ ps; $c_5 = 0.1$, $\tau_5 = 20$ ps. In this case, $F_i(\omega)$ is not as smooth around the τ_0 frequency region. In an actual situation using experimental data, such low-frequency inflections can indicate the presence of a distribution of correlation times for overall tumbling In both these cases, the algorithm is effective at deconvoluting $F_i(\omega)$.

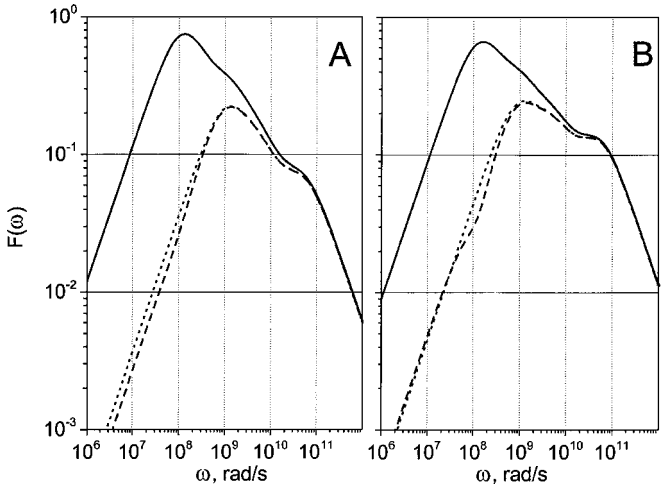

FIG. 5. Spectral densities calculated using the deconvolution algorithm. (A) Solid line: parent function $F(\omega)$ calculated using 5 Lorentzians with $c_0 = 0.7$, $\tau_0 = 8000$ ps; $c_1 = 0.1$, $\tau_1 = 1000$ ps; $c_2 = 0.1$, $\tau_2 = 700$ ps; $c_3 = 0.05$, $\tau_3 = 200$ ps; $c_4 = 0.05$, $\tau_4 = 20$ ps. Dotted line: component of $F(\omega)$ due to internal motions, $F_i(\omega)$. Dashed line: internal motional component $F_i(\omega)$ resulting from minimization using the deconvolution algorithm. (B) Solid line: parent function $F(\omega)$ calculated using 6 Lorentzians with $c_0 = 0.2$, $\tau_0 = 8000$ ps; $c_1 = 0.2$, $\tau_1 = 7000$ ps; $c_2 = 0.2$, $\tau_2 = 6000$ ps; $c_3 = 0.2$, $\tau_3 = 1000$ ps; $c_4 = 0.1$, $\tau_4 = 200$ ps; $c_5 = 0.1$, $\tau_5 = 20$ ps. Dotted line: $F_i(\omega)$. Dashed line: $F_i(\omega)$ resulting from minimization using the deconvolution algorithm.

Additionally, correlation times for overall molecular tumbling can be determined using another property of spectral densities defined in $F3(\omega)$:

$$F3(\omega) = 2(J(0) - J(\omega))/\omega. \quad [20]$$

Assuming that the spectral density can be described as the sum of Lorentzians,

$$F3(\omega) = \sum \frac{2c_i\omega\tau_i^3}{1+\omega^2\tau_i^2}. \quad [21]$$

Although $F3(\omega)$ is similar to $F(\omega)$, correlation times in the numerator are raised to the third power. This dramatically increases contributions from the largest correlation times, i.e., usually those of overall tumbling. In this regard, $F3(\omega)$ primarily contains information about overall tumbling motions. Figure 6A plots $F(\omega)$ (solid line) and $F3(\omega)$ (dashed line) for two Lorentzians with $c_0 = 0.6$, $\tau_0 = 8000$ ps; $c_1 = 0.4$, $\tau_1 = 1000$ ps. A more accurate estimate of τ_0 is given by the $F3(\omega)$ maximum, i.e., $\tau_0 = 1/\omega_{\max}$. This property of $F3(\omega)$, therefore, can be used to better describe low-frequency molecular motions and to help separate out contributions from internal motions.

For peptides and small proteins, internal motions usually contribute most to $F(\omega)$ at higher frequencies than does overall tumbling. This component of $F(\omega)$ is $F_i(\omega)$ in Eq. [16]. The accuracy in determining $F_i(\omega)$ depends on the separation of overall and internal motional correlation times and the number of Lorentzians used to obtain $F(\omega)$. Figure 6B shows the results of fitting $F_i(\omega)$ with $N = 2$, 3, 4 and using calculated ^{13}C NMR relaxation parameters for three spectrometers frequencies ($\nu_H = 250$, 500, and 800 MHz). For this calculation, the following parameters were used:$\tau_0 = 8000$ ps, $c_0 = 0.3$, $\tau_1 = 7000$ ps, $c_1 = 0.3$, $\tau_2 = 1500$ ps, $c_2 = 0.2$, $\tau_3 = 500$ ps, $c_3 = 0.1$, $\tau_4 = 100$ ps, $c_4 = 0.05$, $\tau_5 = 20$ ps, $c_5 = 0.05$, and $R_{ex} = 2\ s^{-1}$. Deconvolution to determine $F_i(\omega)$ was performed using the algorithm described above. Figure 6B demonstrates that by using only two Lorentzians (the Lipari-Szabo approach), $F_i(\omega)$ cannot

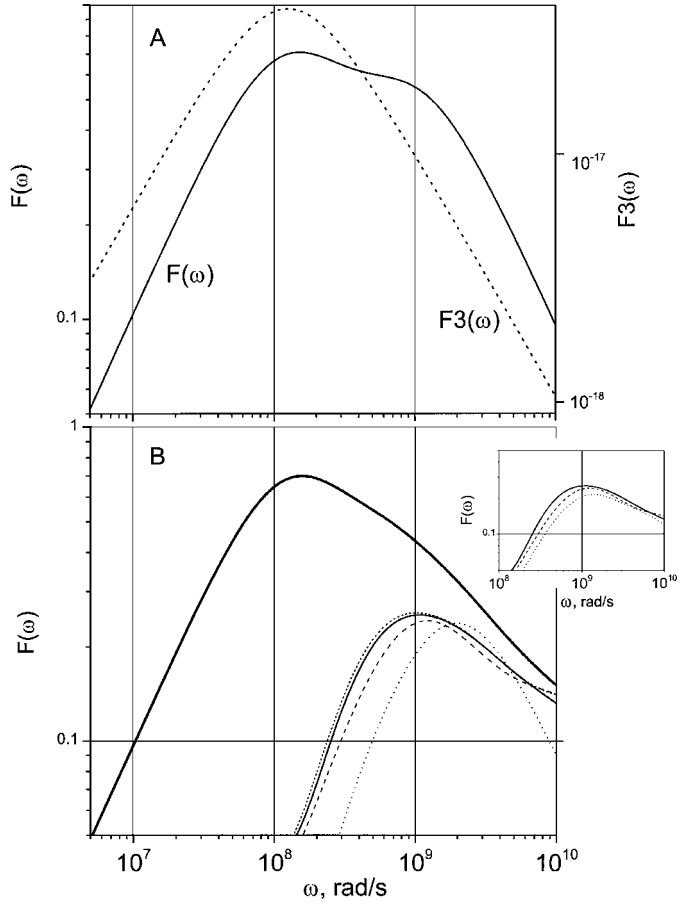

FIG. 6. Spectral densities calculated using Eq. [21]. (A) Parent functions $F(\omega)$ (solid line) and $F3(\omega)$ (dashed line) calculated using two Lorentzians with $c_0 = 0.6$, $\tau_0 = 8000$ ps; $c_1 = 0.4$, $\tau_1 = 1000$ ps. As discussed in the text, $F3(\omega)$ provides information primarily about overall tumbling motions. (B) results of deriving contributions to $F(\omega)$ (solid line) from internal motions, $F_i(\omega)$. Calculations were performed using $N = 2$ Lorentzians (dotted line), $N = 3$ Lorentzians (long dashed line), and $N = 4$ Lorentzians (short dashed line). For these calculations, ^{13}C NMR relaxation parameters calculated for three magnetic fields ($\nu_H = 250$, 500, and 800 MHz) were used. Motional parameters used were $\tau_0 = 8000$ ps, $c_0 = 0.3$; $\tau_1 = 7000$ ps, $c_1 = 0.3$; $\tau_2 = 1500$ ps, $c_2 = 0.2$; $\tau_3 = 500$ ps, $c_3 = 0.1$; $\tau_4 = 100$ ps, $c_4 = 0.05$; $\tau_5 = 20$ ps, $c_5 = 0.05$, and $R_{ex} = 2\ s^{-1}$. Inset shows $F_i(\omega)$ calculated using three Lorentzians and ^{13}C relaxation data acquired at three ($\nu_H = \omega_H/2\pi = 250$, 500, and 800 MHz) (dashed lines) and at two ($\nu_H = 500$ and 800 MHz) (dotted lines) magnetic fields. Solid lines give actual functions $F(\omega)$ and $F_i(\omega)$ derived using the relaxation data.

be determined accurately. On the other hand, using three or more Lorentzians does allow $F_i(\omega)$ to be determined fairly accurately.

For many researchers, performing relaxation experiments at multiple spectrometer frequencies is not possible. Therefore, it is important to understand the influence of using a set number of experiments to fit $F(\omega)$. The inset to Fig. 6B shows $F_i(\omega)$ calculated using experimental ^{13}C relaxation data acquired at three ($\nu_H = 250$, 500, and 800 MHz) and at two ($\nu_H = 500$ and 800 MHz) spectrometer frequencies. It is apparent that even using two magnetic fields (particularly $\nu_H = 800$ MHz) is sufficient to satisfactorily define $F_i(\omega)$.

As discussed above, the error resulting from using the minimization protocol is relatively small. The main source of error in determining $F(\omega)$ rests in the experimental error, i.e., in the NMR relaxation parameters themselves. Since this error depends in part on the frequency ω, it should be minimal in the vicinity of $\omega_i = 0$, ω_C, $\omega_C + \omega_H$, $\omega_C - \omega_H$, and ω_H, which are explicit frequency terms found in the equations for T_1, T_2, and NOE. For proteins where overall correlation times at room temperature are usually in the range 4000 to 7000 ps, the use of ^{13}C relaxation data may be ineffective at determining the low-frequency component of $F(\omega)$, i.e., $F_0(\omega)$. Even at a spectrometer frequency as low as $\nu_C = 62.5$ MHz ($\nu_H = 250$ MHz), the corresponding value of $1/\omega_C$ is only about 2500 ps. This is a typical value for overall tumbling correlation times of peptides at lower temperature, but not usually for proteins larger than about 50 residues. Using ^{15}N NMR relaxation data acquired at $\nu_H = 250$ MHz can be much more effective because $1/\omega_N$ is about 6600 ps, and this is much closer to the typical value of overall correlation times for proteins. For practical consideration, Fig. 7 plots correlation times that correspond to

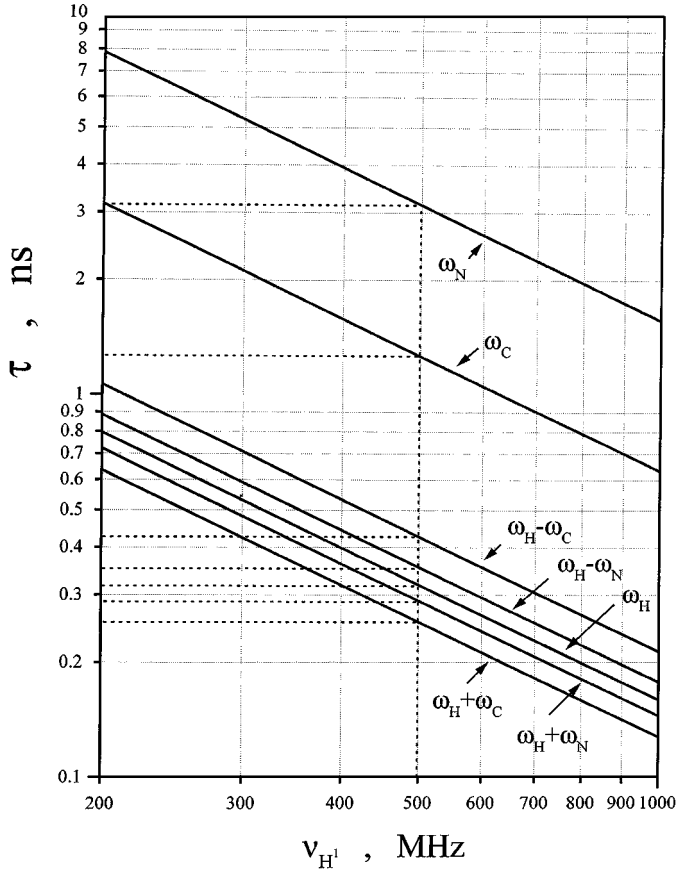

FIG. 7. Correlation times are plotted vs frequencies that correspond to $\omega_{C(N)}$, $\omega_{C(N)} + \omega_H$, $\omega_{C(N)} - \omega_H$ and ω_H for different magnetic field strengths. For simplicity, X-axis values are shown as ν_H. At $\nu_H = 500$ MHz, dashed lines indicate that reliable information can be obtained for correlation times from 260 to 3100 ps.

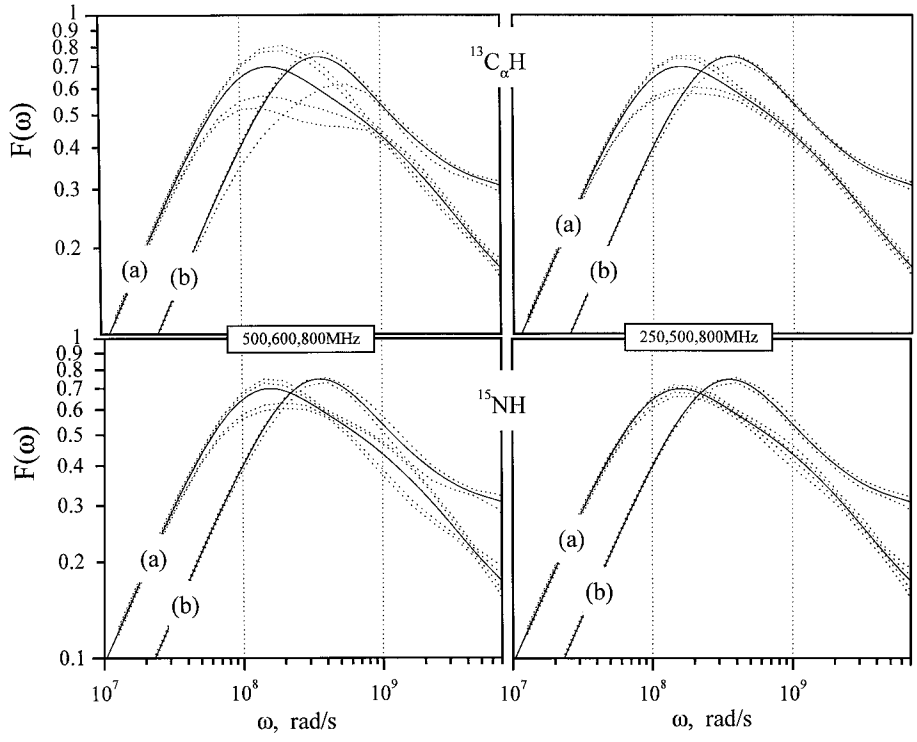

FIG. 8. Curves (a): Error corridors for parent function $F(\omega)$ corresponding to 5 and 2% error in the experimental NMR relaxation parameters (T_1, T_2, NOE) are indicated. Calculations of $F(\omega)$ were performed using 6 Lorentzians with $\tau_0 = 8000$ ps, $c_0 = 0.3$; $\tau_1 = 7000$ ps, $c_1 = 0.3$; $\tau_2 = 1500$ ps, $c_2 = 0.2$; $\tau_3 = 500$ ps, $c_3 = 0.1$; $\tau_4 = 100$ ps, $c_4 = 0.05$; $\tau_5 = 20$ ps, $c_5 = 0.05$. The chemical exchange term, R_{ex}, was set equal to 2 s^{-1}. Calculated ^{13}C and ^{15}N NMR relaxation parameters were analyzed for two sets of magnetic field strengths: $\nu_H = 250$, 500, 800 MHz and $\nu_H = 500$, 600, and 800 MHz. Curves (b): Corridors of error for $F(\omega)$ calculated using three Lorentzians defined by $\tau_0 = 3000$ ps, $c_0 = 0.7$; $\tau_1 = 500$ ps, $c_1 = 0.1$; $\tau_2 = 100$ ps, $c_2 = 0.2$; and $R_{ex} = 2\,s^{-1}$.

frequencies $\omega_{C(N)}$, $\omega_{C(N)} + \omega_H$, $\omega_{C(N)} - \omega_H$ and ω_H, as a function of spectrometer ^1H frequency, ν_H. This illustration indicates that only internal motions exhibiting correlation times of 100 ps or greater can be derived. In fact, using data acquired only at ν_H =500 MHz yields the most reliable information for correlation times between 260 and 3100 ps.

To better assess the influence of experimental error on $F(\omega)$, calculations were performed at every point on $F(\omega)$ that corresponds to Gaussian distributions of the experimental NMR relaxation parameters T_1, T_2, NOE. Results of this calculation are illustrated in Fig. 8, which illustrates the corridor of error in $F(\omega)$ given by

$$\frac{1}{N}\sum\left(\frac{P_i - P_{i0}}{\mathrm{err}_i}\right)^2 < 1. \qquad [22]$$

P_i are values of relaxation parameters (T_1, T_2, NOE) that have been calculated for c, and τ where inequality [22] is true. P_{i0} are values of relaxation parameters that give the exact solution. N is the number of experiments. Errors, err_i, are given as standard deviations for the distribution of experimental parameters. The calculation was performed for $\mathrm{err}_i = 0.05$ and for $\mathrm{err}_i = 0.02$. The c and τ parameters that define $F(\omega)$ are $\tau_0 = 8000$ ps, $c_0 = 0.3$, $\tau_1 = 7000$ ps, $c_1 = 0.3$, $\tau_2 = 1500$ ps, $c_2 = 0.2$, $\tau_3 = 500$ ps, $c_3 = 0.1$, $\tau_4 = 100$ ps, $c_4 = 0.05$, $\tau_5 = 20$ ps, $c_5 = 0.05$, with $R_{ex} = 2s^{-1}$. ^{13}C and ^{15}N NMR relaxation data were analyzed for two sets of spectrometer frequencies: (1) $\nu_H = 250$, 500, and 800 MHz and (2) $\nu_H = 500$, 600, and 800 MHz. The corridors of error can be interpreted as regions wherein $F(\omega)$ is given with 67% probability. As expected, the narrowest corridors of error are observed at points close to 0, $\omega_{C(N)}$, $\omega_{C(N)} + \omega_H$, $\omega_{C(N)} - \omega_H$, and ω_H. As mentioned above, it is clear that using ^{15}N relaxation data and, therefore, lower spectrometer frequencies allows a more accurate definition of the low-frequency region of $F(\omega)$ that is dominated by contributions from overall molecular tumbling motions.

Figure 8 also shows corridors of error for $F(\omega)$ calculated using three Lorentzians defined by $\tau_0 = 3000$ ps, $c_0 = 0.7$, $\tau_1 = 500$ ps, $c_1 = 0.1$, $\tau_2 = 100$ ps, $c_2 = 0.2$, and $R_{ex} = 2\,s^{-1}$. The calculation was performed for an $\mathrm{err}_i = 0.03$. Use of a smaller overall tumbling time shifts the curves to higher frequency (see curves shifted to the right in the figure). Note that in this case, errors are much smaller, and even using data acquired at high field allows $F(\omega)$ to be determined quite accurately over a wider frequency range. In this regard, overall tumbling parameters can only be determined accurately for peptides and small proteins

using ^{13}C NMR relaxation data acquired at high temperatures where overall correlation times are less than about 4000 ps. As already mentioned, ^{15}N NMR relaxation data that reaches lower frequencies should be used with larger, slower tumbling molecules.

The extent to which experimental errors contribute to $F(\omega)$ can be estimated by considering that P_k are experimental parameters (T_1, T_2, NOE) acquired at various spectrometer frequencies and R_k^i are relaxation parameters obtained for a randomly generated set of c_i and τ_i with $F^i(\omega)$ being the function $F(\omega)$ for a given set of c_i, τ_i, such that

$$\chi_i^2 = \sum_k \left(\frac{P_k^i - R_k}{\sigma_k} \right)^2, \qquad [23]$$

where σ_k are standard deviations (errors) from experimental parameters, P_k. $F(\omega)$, calculated by using the Monte Carlo method, is given by

$$F(\omega) = \frac{\sum F^i(\omega) p_i}{\sum p_i}, \qquad [24]$$

where

$$p_i = \exp(-\chi_i^2/2). \qquad [25]$$

Since the speed and accuracy of this calculation depends upon the selection of c_i, τ_i, it is better to perform summations of $F^i(\omega)$ over small values of χ_i^2 where a Gaussian distribution for $F^i(\omega)$ may be assumed. Therefore, this approach does not allow values of c_i, τ_i to be derived explicitly because there are numerous combinations of these parameters that yield very similar values of $F(\omega)$. Of utmost importance to this discussion is that the function $F(\omega)$ itself can be determined accurately. For all intents and purposes, the corridors of error in $F(\omega)$ depend only on experimental errors arising from the relaxation data, and using relaxation data acquired at multiple spectrometer frequencies substantially narrows this corridor of error.

Application to an α-Helix-Forming Peptide

$^{13}C_\alpha H$ and ^{15}NH relaxation data were acquired on the hydrophobic staple, α-helix-forming peptide GFSKAELAKARA-AKRGGY (*32*). The N-terminal part of the peptide contains a hydrophobic staple formed primarily from F2 and L7 that stabilizes the helix-forming part of the peptide running from A5 through A13. This structure is most stable at lower temperature, i.e., 5°C, and in the presence of TFE (*31*). Relaxation data on this peptide have been acquired and include spin–lattice (T_1) and spin–spin (T_2) relaxation times, as well as heteronuclear NOEs, {^{1}H}–^{13}C and {^{1}H}–^{15}N, measured at four Larmor precession frequencies (^{1}H frequencies of 250, 500, 600, and 800 MHz) and at temperatures between 5 and 30°C. Measurements were performed in water and in water/TFE (60/40, v/v). Examples of the raw data have been presented elsewhere (*19*). With these data, $F(\omega) = 2\omega J(\omega)$ and the corresponding spectral density functions, $J(\omega)$, were determined over the frequency range $0 < \omega < 6.28 \times 10^9$ rad/s using Monte Carlo minimization.

Figures 9 and 10 illustrate results of calculating $F(\omega)$ for $C_\alpha H$ and NH backbone bonds in the α-helix-forming peptide in water and in water/TFE as a function of temperature. Errors in determining $F(\omega)$ were calculated using Eq. [24]. These errors are indicated with vertical bars only for residue A10 in Figs. 9 and 10. Similar errors are observed with other residues. Note that the error in $F(\omega)$ increases at lower and higher motional frequencies where the actual NMR spectrometer frequencies limit the experimentally accessible frequency range for ^{13}C and ^{15}N nuclei. Nevertheless, the frequency range shown does cover three decades from 10 to 10,000 MHz (10 GHz). Solid circles on the curve represent frequencies $\omega_{C(N)}$ and $\omega_{C(N)} \pm \omega_H$ at which experimental data were collected. The point at $J(\omega) = 0$ is not shown on this $F(\omega)$ plot due to the use of the log scale. This has been done only for residues F2, A5, L7, and A8 of the peptide at 5°C.

Because this is a new approach, one might ask how accurate is it in correctly reporting motional frequencies. Three observations in particular render confidence in this approach. Firstly, the inverse of the X-axis position of the $F(\omega)$ maxima at low-frequency essentially corresponds to overall tumbling correlation times derived using the Lipari–Szabo and other motional models (*19*). For example, for the peptide in water at 5°C, the L7 ^{15}NH group gives a $F(\omega)$ maxima at about 500 MHz, the inverse of which is the motional correlation time of 2 ns. Using the Lipari–Szabo model free approach and these same relaxation data, Idiyatullin *et al.* (*19*) derived a correlation time of 1.8 ns. Similar comparisons can be made with other residues. Secondly, $F(\omega)$ curves demonstrate a smooth transition with changes in temperature and their maxima shift to lower frequency (to the left in the figure) as the temperature is decreased. Physically, this should be the case because these maxima are mostly attributable to overall molecular tumbling motions that should become slower at lower temperature. Thirdly, addition of TFE has the same effect on the overall tumbling time as does lowering temperature. This too is expected because TFE increases solution viscosity and, therefore, should yield larger overall tumbling correlation times and shift $F(\omega)$ maxima to lower frequency.

Although $F(\omega)$ is generally dominated by overall tumbling motions, contributions from faster internal motions are often apparent on the high-frequency side of these curves. In some instances, a shoulder or a minor second maxima is observed. In others, the function merely appears asymmetric or broadened on the high-frequency side. The later case is mostly observed for $^{13}C_\alpha H$ and ^{15}NH internal motions of the peptide in water alone, and only for F2 is a high-frequency component readily observable. For F2, $F(\omega)$ becomes rather flat at higher frequencies, indicating internal motional contributions

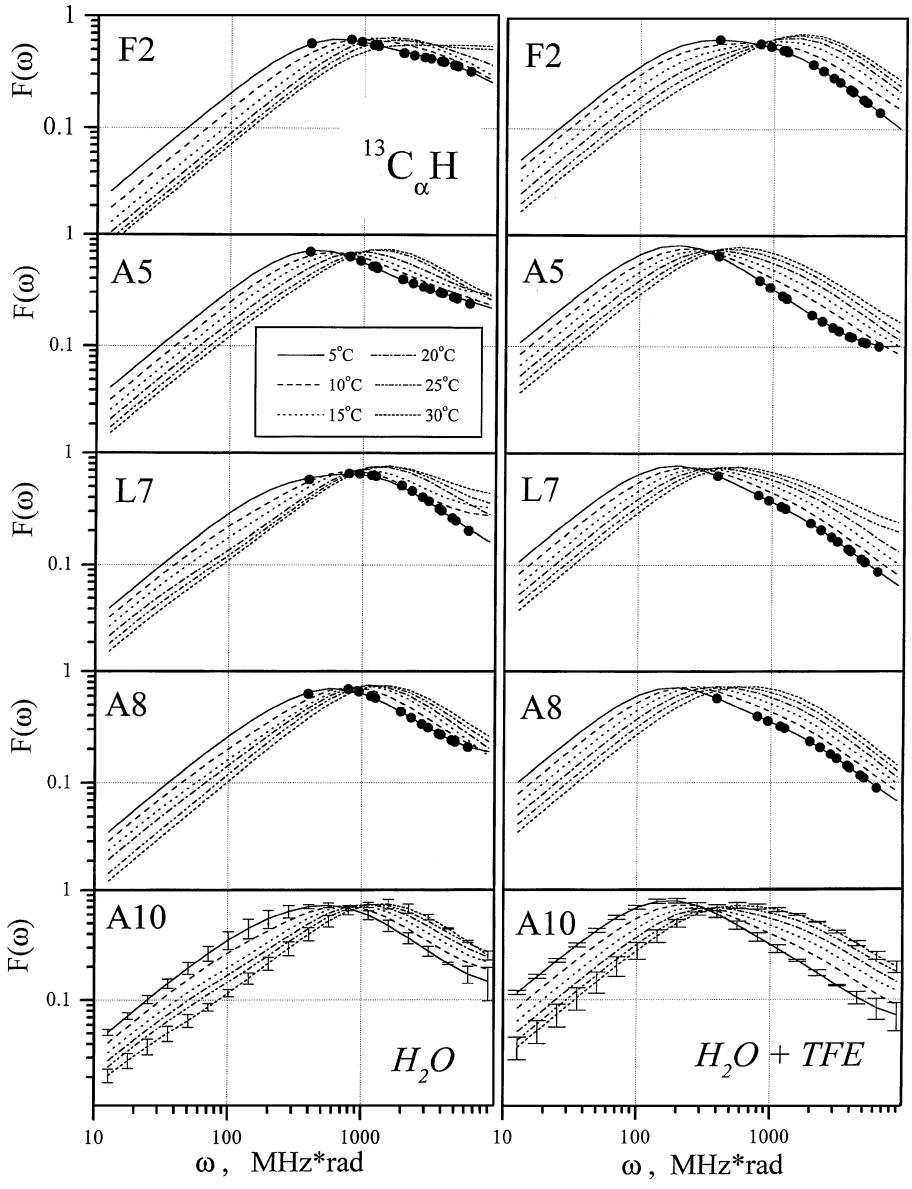

FIG. 9. Functions $F(\omega)$ have been calculated using experimental data for five $^{13}C_\alpha H$ backbone bonds (residues F2, A5, L7, A8, and A10) in the α-helix-forming peptide in water and in water/TFE. Data are shown for temperatures from 5 to 30°C. Solid circles on the curve represent frequencies $\omega_{C(N)}$ and $\omega_{C(N)} \pm \omega_H$ at which experimental data were collected. The value at $J(\omega) = 0$ is not shown on this $F(\omega)$ plot due to the use of the log scale.

with correlation times from 100 ps to 1 ns. These relatively faster motions are related to the fact that F2 is more internally mobile by virtue of it being at the N-terminus. In fact, for the F2 ^{15}NH group at higher temperatures, internal motions contribute more to the spectral density function than do overall tumbling motions.

In water/TFE, on the other hand, where slower overall tumbling of the molecule shifts $F(\omega)$ maxima to lower frequencies, shoulders or minor second maxima become apparent for most $^{13}C_\alpha H$ and ^{15}NH groups. As mentioned above, slower overall molecular tumbling should lead to better separation of overall tumbling and internal motional correlation times as these data attest. From the position of these shoulders or minor second maxima, internal motional frequencies are estimated to range from a few hundred picoseconds to near one nanosecond. For $^{13}C_\alpha H$ groups of F2, L7, and A8 at 5°C, a high-frequency shoulder is positioned at about 1000 to 2000 MHz, whereas for ^{15}NH groups of these same residues, the high-frequency side of $F(\omega)$ shows more of a second maxima centered at about 500 MHz. As with the peptide in water, in water/TFE internal motions of N-terminal residue F2 contribute to $F(\omega)$ more than overall tumbling motions and more than do internal motions of other residues within the more well-folded α-helical part of the peptide (residues A5 to A13).

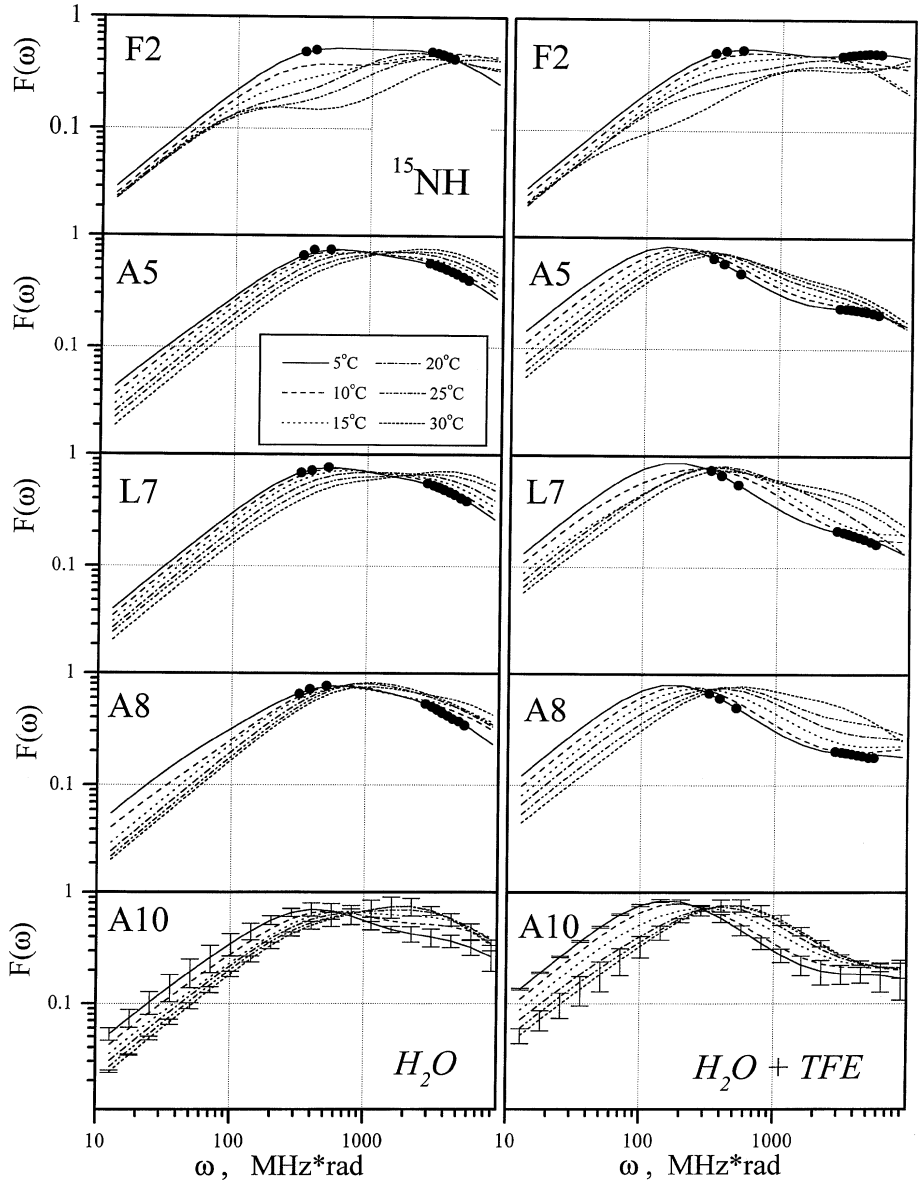

FIG. 10. Functions $F(\omega)$ have been calculated using experimental data for five ^{15}NH backbone bonds (residues F2, A5, L7, A8, and A10) in the α-helix-forming peptide in water and in water/TFE. Data are shown for temperatures from 5 to 30°C. Solid circles on the curve represent frequencies $\omega_{C(N)}$ and $\omega_{C(N)} \pm \omega_H$ at which experimental data were collected. The value at $J(\omega) = 0$ is not shown on this $F(\omega)$ plot due to the use of the log scale.

To more accurately determine internal motional frequencies, $F(\omega)$ has been deconvoluted into components for overall tumbling, $F_o(\omega)$, and for internal motions, $F_i(\omega)$, using the deconvolution procedure described in the previous section. The accuracy of deconvolution, of course, depends on the separation of internal motional and overall tumbling correlation times. Errors are smaller when contributions from $F_i(\omega)$ and the difference between overall tumbling and internal motional correlation times are relatively large. In water, overall tumbling and internal motional correlation times are closer together than in water/TFE and contributions from $F_i(\omega)$ are relatively small, resulting in a less accurate determination of $F_i(\omega)$. Nevertheless, from the shape of $F_i(\omega)$, it may be concluded that $F_o(\omega)$ in water cannot be described by a single Lorentzian, particularly at low temperature, indicating the presence of a broad distribution of overall correlation times, which, in turn, is related to the presence of a relatively broad distribution of rapidly interconverting species of folded and unfolded peptide.

Because contributions from $F_i(\omega)$ and the difference between overall tumbling and internal motional correlation times are larger in water/TFE wherein the peptide is also more folded, only these data will be presented. To exemplify results from

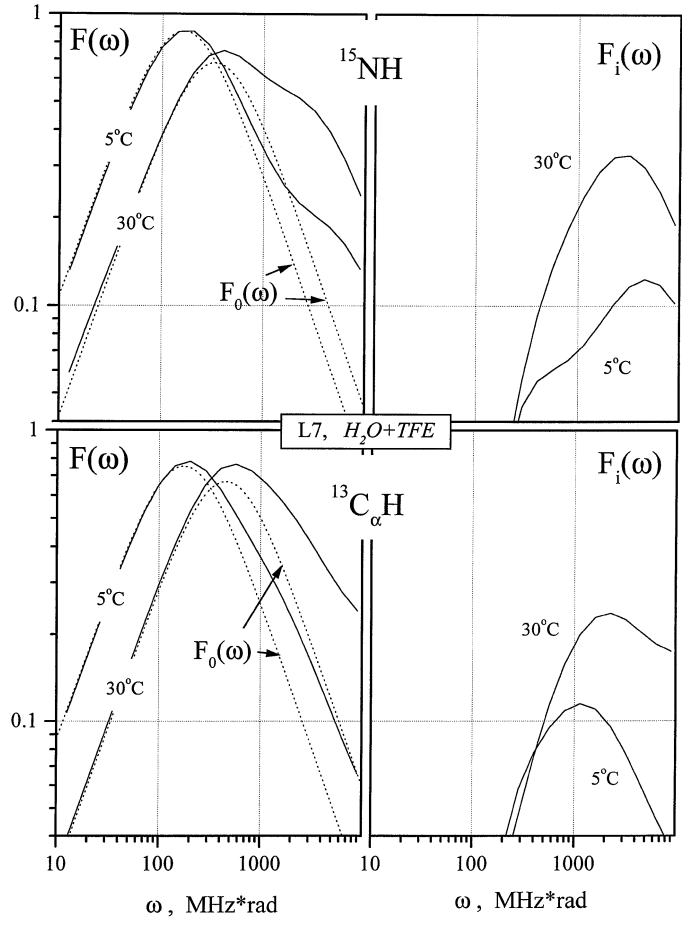

FIG. 11. Deconvolution procedure for ^{15}NH and $^{13}C_\alpha$H groups of residue L7 from the α-helix-forming peptide in water/TFE. The deconvolution of parent functions $F(\omega)$ (solid lines) into component functions for overall tumbling, $F_o(\omega)$, and internal motions, $F_i(\omega)$, are shown for two temperatures, 5 and 30°C, as indicated. Component functions $F_o(\omega)$ and $F_i(\omega)$ are plotted in panels on the left (dotted lines) and on the right (solid lines), respectively.

this deconvolution procedure, Fig. 11 plots the parent function $F(\omega)$ and derived $F_o(\omega)$ and $F_i(\omega)$ components for L7 $^{13}C_\alpha$H and ^{15}NH groups of the peptide in water/TFE at 5 and 30°C. For these two temperatures, the parent function $F(\omega)$ is plotted as solid lines and the component for overall tumbling, $F_o(\omega)$, is plotted as dotted lines. $F_i(\omega)$ components are plotted in separate panels at the right in this figure. Within this frequency regime, $F_i(\omega)$ indicates that internal motional correlation times are distributed around 200 to 300 ps for the NH group and around 500 to 700 ps for the C_αH group. As shown in Fig. 12, results are, for the most part, similar for other residues (A5, A8, and A10) within the helical segment of the peptide. This is more true for C_αH groups. For NH groups of A8 and A10, however, $F_i(\omega)$ distributions are on the rise over this frequency range, but appear to be peaking around a smaller correlation time near 100 ps. In a few cases, $F_i(\omega)$ is not very well defined. For example, for A5 C_αH at 5°C, $F_i(\omega)$ is rather flat, not highly populated and tends to grow only at the highest frequencies shown. This could occur because the relaxation data acquired under these specific conditions were not optimal or that the contribution from $F_i(\omega)$ to $F(\omega)$ was so small as not to be accurately definable. Since the experimental data look as good as those acquired under other conditions, the later possibility is the more probable. For F2, the deconvolution procedure produced a reasonable $F_i(\omega)$ distribution for the $^{13}C_\alpha$H group, but not for the ^{15}NH group (data not shown). In Fig. 9 it was already apparent that internal motions of the F2 ^{15}NH group occured primarily at frequencies higher than those accessible experimentally, i.e., correlation times less than 100 ps. For the F2 $^{13}C_\alpha$H group, internal motional correlation times were about the same as those for $^{13}C_\alpha$H groups within the helix segment.

One of the main observations that arises from these correlation time distributions is that internal motions are somewhat faster

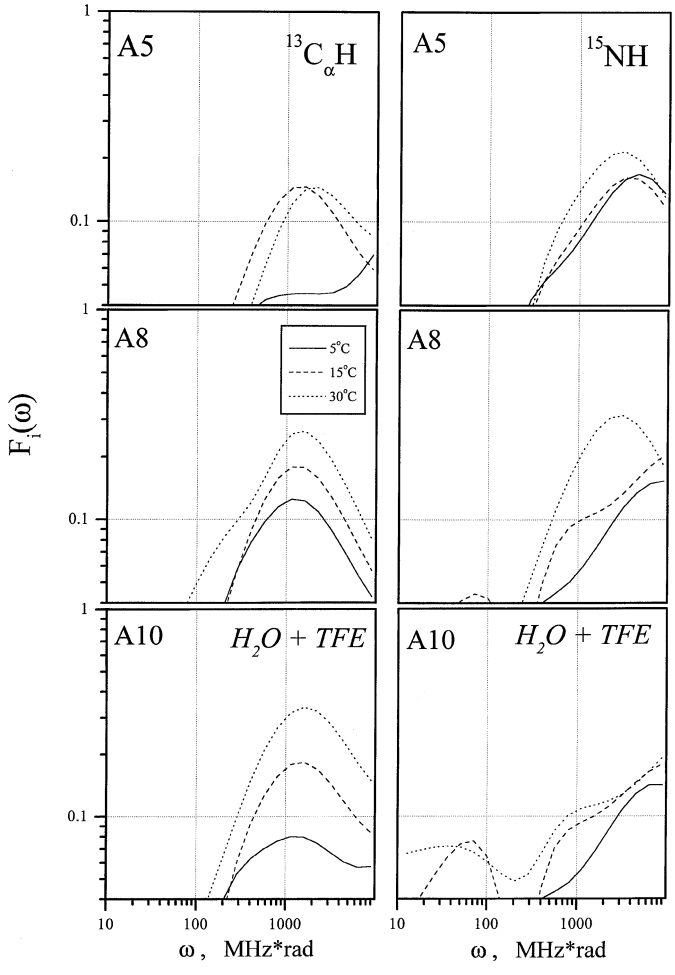

FIG. 12. Deconvolution procedure for ^{15}NH and $^{13}C_\alpha$H groups of residues A5, A8, and A10 from the α-helix-forming peptide in water/TFE. As discussed in the text, the deconvolution of parent functions $F(\omega)$ into component functions for overall tumbling, $F_o(\omega)$, and internal motions, $F_i(\omega)$, are shown for three temperatures, 5, 15, and 30°C, as indicated in the figure. Only component functions $F_i(\omega)$ are shown.

for NH bond vectors than for $C_\alpha H$ bond vectors. Slower internal motions for backbone $C_\alpha H$ groups are probably related to the fact that $C_\alpha H$ bond motions are more restricted than are NH bond motions. Idiyatullin *et al.* (*19*) have shown that for this same peptide in water/TFE, amplitudes of rotations in helix residues A5, L7, A8, and A10, are, on average, smaller for $C_\alpha H$ bonds (about 15°) than for NH bonds (about 25°). $C_\alpha H$ bond motions are influenced by the presence of the amino acid side chain, which may act to dampen $C_\alpha H$ bond motions. Depending on the potential energy landscape for overall internal motions of this peptide, greater motional constraints of one vector relative to another could result in lower motional frequencies as observed here for $C_\alpha H$ groups. It is also possible that the component for overall tumbling, $F_o(\omega)$, also contains contributions from slower internal motions that fall coincidently within that component of the parent function $F(\omega)$. However, for this to occur, the distribution would have to be as symmetric as $F_o(\omega)$, which is probably unlikely.

Internal motions of backbone bond vectors occurring on the time scale 100 ps to 1 ns are not uncommon. Using ^{15}N NMR relaxation data, Clore *et al.* (*33*) found that 32 residues of the protein interleukin-1β display motions on a time scale of 0.5 to 4 ns, slightly less than the overall molecular rotational correlation time of 8.3 ns. Internal motions occurring on the nanosecond time scale have also been observed using other techniques. For example, analysis of fluorescence data on the peptide melittin revealed anisotropic internal motions of the single tryptophan on a time scale of 140 to 720 ps (*34*), and Tamura *et al.* (*35*) used solid state deuterium NMR to demonstrate that the methyl group axes of three methionines in the Streptomyces subtilisin inhibitor protein undergo internal motions with correlation times between 0.1 and 10 ns.

Application to a Compactly Folded Protein

As discussed and exemplified above, slower overall molecular tumbling of the helix-forming peptide in TFE relative to water led to a shift in the $F(\omega)$ maximum to lower frequency and better separation of overall tumbling and internal motional correlation times. In this section, this new approach to visualizing spectral density functions is exemplified using 2D NMR $^{13}C/^{15}N$ HSQC-derived relaxation data (Chang *et al.*, data and complete analysis to be published elsewhere) on a larger, compactly folded protein, the 138-residue regulatory protein, component B (MMOB), from methane monooxygenase (*20*). The NMR-derived solution structure of MMOB shows the presence of a well-ordered core region (residues 36–126) and highly mobile, disordered N- (residue 1–35) and C-terminal (residues 127–138) regions (*20*). The compactly folded core region of MMOB is composed of two folding domains: one $\beta\alpha\beta\beta$ and one $\beta\alpha\alpha\beta\beta$. To exemplify the new approach on this system, Fig. 13 (left panels) plots $F(\omega)$ for ^{15}NH and $^{13}C_\alpha H$ motional vectors of five residues, A26, D71, K72, F75, and A80. Solid circles on the curve represent frequencies $\omega_{C(N)}$ and $\omega_{C(N)} \pm \omega_H$ at which experimental data were collected. $J(\omega) = 0$ is another point on the $F(\omega)$ curve, but its value is not shown on this plot due to the use of the log scale. Residue A26 is part of the mobile and structurally disordered N-terminal segment, and the other four residues are part of β-strands 2 (residues 67–72) and 3 (residues 75–80). These two β-strands are part of the anti-parallel β-sheet in the $\beta\alpha\beta\beta$ domain. Figure 13 (right panels) also plots the function $F_i(\omega)$ that was derived by deconvolution of $F(\omega)$ as discussed in the previous section.

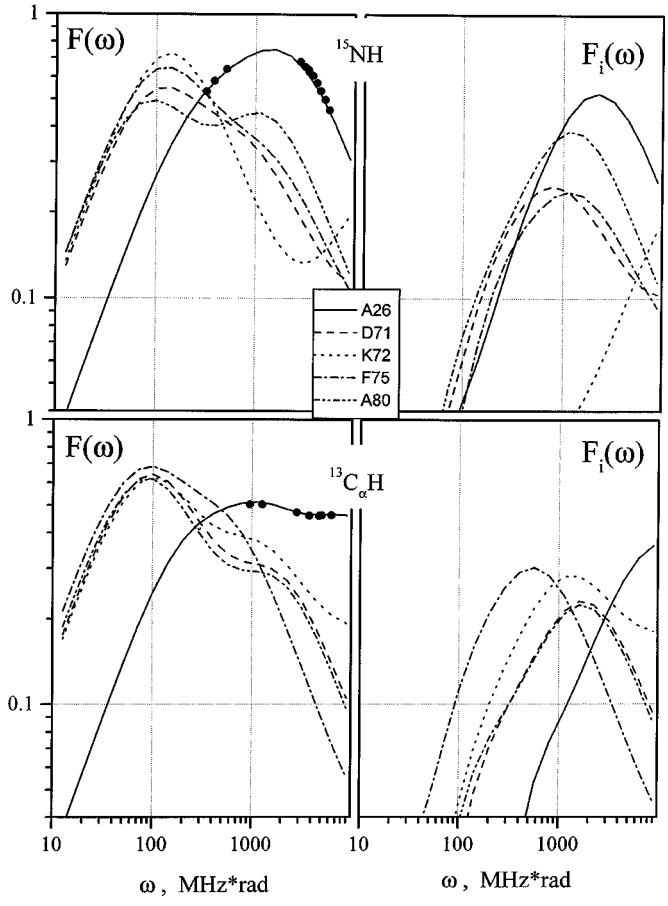

FIG. 13. Functions $F(\omega)$ have been calculated using experimental data for five $^{13}C_\alpha H$ and ^{15}NH backbone bonds (residues A26, D71, K72, F75, and A80) in the compactly folded, 138- residue protein MMOB in water at 30°C. These are displayed in the left-hand panels, and solid circles on the solid curves represent frequencies $\omega_{C(N)}$ and $\omega_{C(N)} \pm \omega_H$ at which experimental data were collected. The value at $J(\omega) = 0$ is not shown on this $F(\omega)$ plot due to the use of the log scale. The deconvolution procedure has been applied to ^{15}NH and $^{13}C_\alpha H$ groups of these same residues of MMOB. As discussed in the text, the parent functions, $F(\omega)$, have been deconvoluted into component functions for overall tumbling, $F_o(\omega)$, and internal motions, $F_i(\omega)$. The component functions $F_i(\omega)$ are shown in the right-hand panels.

First, note that in Fig. 13 the low-frequency maxima of $F(\omega)$ for β-sheet residues D71, K72, F75, and A80 are shifted to lower frequencies compared to those for the helix-forming peptide in water. This is expected because MMOB is larger and more compactly folded than the peptide. From the inverse of

the frequency at the maximum of $F(\omega)$, an average overall tumbling correlation time, τ_o, of 9 ns can be estimated for MMOB. Using the Lipari–Szabo approach, the average τ_o is essentially the same, 8.3 ns. Moreover, because MMOB is a larger system, slower and faster motions are better seperated. For example, for $^{13}C_\alpha H$ groups of residues D71 and A80 and for the ^{15}NH group of A80, two maxima are clearly differentiable on the high-frequency side of $F(\omega)$. From the position of these second maxima, internal motional frequencies are estimated to range from several hundred picoseconds to near one nanosecond. For other $^{13}C_\alpha H$ and ^{15}NH groups, high-frequency shoulders are positioned at or near the one-nanosecond mark. In addition, from the distribution of motions in $F(\omega)$, contributions from internal motions appear to be nearly the same as from overall tumbling. A26 was chosen to exemplify a more internally mobile residue. In this case, $F(\omega)$ is weighted more on the high-frequency side, indicating the greater importance of internal motions to spectral density functions for $^{13}C_\alpha H$ and ^{15}NH groups of A26.

To more accurately determine internal motional frequencies, $F(\omega)$ has been deconvoluted into components for overall tumbling, $F_o(\omega)$, and for internal motions, $F_i(\omega)$, using the deconvolution procedure described in the previous sections. $F_i(\omega)$ is shown in panels at the right in Fig. 13. Compared to data on the helix-forming peptide presented above, these data on MMOB yield more accurate $F_i(\omega)$ curves because of the better separation of internal motional and overall tumbling correlation times. Within this frequency regime, $F_i(\omega)$ indicates that internal motional correlation times for D71, F75, and A80, for example, are distributed around 1 ns for their NH groups and around 800 ps for their $C_\alpha H$ groups. Interestingly, internal motions for NH bond vectors are somewhat slower than for $C_\alpha H$ bond vectors. The opposite was observed with the helix-forming peptide. Slower internal motions for backbone NH groups may be related to the fact that these NHs in MMOB are involved in hydrogen bonding within the β-sheet, and therefore these NH motions are somewhat more restricted than are their $C_\alpha H$ bond motions. On the other hand, the same trend is observed with A26, which is not part of the well-folded core of MMOB. With A26, however, the situation is complicated by the fact that internal motions appear to contribute more to the spectral density functions and internal and overall motional correlation times are less well separated. In this regard, the exact reason(s) for the occurrence of internal motions of NH groups on a time scale slightly slower than that of $C_\alpha H$ groups is (are) unknown. In any event, this new approach provides a relatively good way for deriving internal motional correlation time distributions in peptides and proteins.

CONCLUSIONS

Although standard, commonly used analyses of NMR relaxation data, e.g., the Lipari–Szabo approach, provide correlation times for overall molecular tumbling, τ_o, and for internal motions, τ_i, along with an order parameter, S^2, only the correlation time for overall tumbling and the order parameter can be determined reasonably accurately, and at that, only if the molecule is globular and symmetrically shaped. In this regard, the best that can be derived from such analyses in terms of internal motions is some indication of internal motional restriction from the order parameter, but not an accurate determination of the motional frequencies themselves. In this regard, using this new approach, i.e., the function $F(\omega) = 2\omega J(\omega)$, to describe molecular motions has several advantages. For one, it provides a relatively simple visualization of the distribution of correlation times for molecular motions and their contributions to the spectral density function, and it is fairly straightforward to separate overall molecular tumbling and internal motions occurring on the picosecond-to-nanosecond time scales. Furthermore, this approach demonstrates a low sensitivity to the number of Lorentzians used to describe these molecular motions. The examples of the α-helix-forming peptide and well-folded protein MMOB presented here indicate that as the overall tumbling correlation time (molecular size) increases, i.e., the system becomes larger, the generally higher frequency internal motional components become better defined in $F(\omega)$ and therefore more accurately determinable.

ACKNOWLEDGMENTS

This work was supported by research grants from the National Institutes of Health (GM-58005) and the National Science Foundation (MCB-9729539) and benefitted from use of the high field NMR facility at the University of Minnesota.

REFERENCES

1. L. G. Werbelow and D. M. Grant, Intramolecular dipolar relaxation in multispin systems, *Adv. Magn. Reson.* **9,** 189–299 (1977).
2. V. A. Daragan and K. H. Mayo, Motional model analyses of protein and peptide dynamics using ^{13}C and ^{15}N NMR relaxation, *Prog. NMR Spectrosc.* **32,** 63–105 (1997).
3. J. W. Peng and G. Wagner, Mapping of spectral density functions using heteronuclear NMR relaxation measurements, *J. Magn. Reson.* **98,** 308–332 (1992).
4. J. P. Peng and G. Wagner, Mapping of the spectral densities of N–H bond motions in egline *c* using heteronuclear relaxation experiments, *Biochemistry* **31,** 8571–8586 (1992).
5. J. P. Peng and G. Wagner, Frequency spectrum of NH bonds in eglin c from spectral density mapping at multiple fields, *Biochemistry* **34,** 16,733–16,752 (1995).
6. N. A. Farrow, O. Zhang, A. Szabo, D. A. Torchia, and L. E. Kay, Spectral density function mapping using ^{15}N relaxation data exclusively, *J. Biomol. NMR* **6,** 153–162 (1995).
7. J. F. Lefevre, K. T. Dayie, J. W. Peng, and G. Wagner, Internal mobility in the patially folded DNA binding and dimerization domains of GAL4: NMR analysis of the N–H spectral density function, *Biochemistry* **35,** 2674–2686 (1996).
8. G. Lipari and A. Szabo, Model-free approach to the interpretation of nuclear magnetic resonance relaxation in macromolecules. I. Theory and range of validity, *J. Am. Chem. Soc.* **104,** 4546–4559 (1982).
9. G. Lipari and A. Szabo, Model-free approach to the interpretation of nuclear magnetic resonance relaxation in macromolecules. II. Analysis of experimental results, *J. Am. Chem. Soc.* **104,** 4559–4570 (1982).

10. R. E. London and J. Avitable, ^{13}C-{^{1}H} NOE and ^{13}C spin lattice relaxation in molecules undergoing multiple internal rotations, *J. Chem. Phys.* **65,** 2443–2450 (1976).

11. G. Lipari and A. Szabo, Effect of librational motion on fluorence depolarization and NMR relaxation in macromolecules and membranes, *Biophys. J.* **30,** 489–506 (1980).

12. G. Lipari and A. Szabo, Pade approximants to correlation function for restricted rotational diffusion, *J. Chem. Phys.* **75,** 2971–2976 (1981).

13. G. M. Clore, A. Szabo, A. Bax, L. E. Kay, P. C. Driscoll, and A. M. Gronenborn, Deviations from the simple two-parameter model-free approach to the interpretation of nitrogen-15 nuclear magnetice relaxation of proteins, *J. Amer. Chem. Soc.* **112,** 4989–4991 (1990).

14. V. A. Daragan and K. H. Mayo, Using the model free approach to analyze NMR relaxation data in cases of anisotropic molecular diffusion, *J. Phys. Chem.* **103,** 6829–6843 (1999).

15. R. King and O. Jardetzky, A general formalism for the analysis of NMR relaxation measuremenmts on systems with multiple degree of freedom, *Chem. Phys. Lett.* **55,** 15–18 (1978).

16. A. A. Ribeiro, R. King, C. Restivo, and O. Jardetzky, An approach to the mapping of internal motions in proteins. Analysis of ^{13}C NMR relaxation in bovine pancreatic trypsin inhibitor, *J. Am. Chem. Soc.* **102,** 4040–4051 (1980).

17. V. A. Daragan and K. H. Mayo, A novel model-free analysis of 13C-NMR relaxation of alanine methyl side-chain motions in peptides, *J. Magn. Reson. B* **110,** 164–175 (1996).

18. E. Atherton and R. C. Sheppard, "Solid Phase Peptide Synthesis: A Practical Approach." IRL Press, Oxford (1989).

19. D. Idiyatullin, A. Krushelnitsky, I. Nesmelova, F. Blanco, V. A. Daragan, L. Serrano, and K. H. Mayo, Internal motional amplitudes and correlated bond rotations in an α-helix peptide derived from ^{13}C- and ^{15}N-NMR relaxation, *Protein Sci.* **9,** 2118–2127 (2000).

20. S.-L. Chang, B. J. Wallar, J. D. Lipscomb, and K. H. Mayo, Solution structure of component B from methane Monooxygenase derived through heteronuclear NMR and molecular modeling, *Biochemistry* **38,** 5799–5812 (1999).

21. A. J. Shaka, P. B. Barker, and R. Freeman, Computer-optimized decoupling scheme for wideband applications and low-level operation, *J. Magn. Reson.* **64,** 547–552 (1985).

22. N. Farrow, R. Muhandiram, A. Singer, S. Pascal, C. Kay, G. Gish, S. Shoelson, T. Pawson, J. Forman-Kay, and L. Kay, Backbone dynamics of a free and phosphopeptide-complexed Src homology 2 domain studied by ^{15}N NMR relaxation, *Biochemistry* **33,** 5984–6003 (1994).

23. T. Tokuhiro and G. Fraenkel, Modulation of spin echoes in multi-half-spin systems. Closed formulas of Carr-Purcell spin echoes in several A_aBX_x systems, *J. Chem. Phys.* **49,** 3998–4008 (1968).

24. A. J. Shaka, J. Keeler, T. Frenkiel, and R. Freeman, An improved sequence for broadband decoupling: WALTZ-16, *J. Magn. Reson.* **52,** 335–338 (1983).

25. V. A. Daragan, M. A. Kloczewiak, and K. H. Mayo, ^{13}C nuclear magnetic resonance relaxation-derived ϕ, Ψ bond rotational energy barriers and rotational restrictions for glycine $^{13}C_\alpha$ methylenes in a GXX-repeat hexadecapeptide, *Biochemistry* **32,** 10,580–10,590 (1993).

26. J. L. Markley, W. J. Horsley, and M. P. Klein, Spin-lattice relaxation measurements in slowly relaxing complex spectra, *J. Chem. Phys.* **55,** 3604–3605 (1971).

27. S. Zinn-Justin, P. Berthault, M. Guenneugues, and H. Desvaux, Off-resonance rf fields in heteronuclear NMR: Application to the study of slow motions, *J. Biomol. NMR* **10,** 363–372 (1997).

28. F. A. A. Mulder, R. A. deGraaf, R. Kaptein, and R. Boelens, An off-resonance rotating frame relaxation experiment for the investigation of macromolecular dynamics using adiabatic rotations, *J. Magn. Reson.* **131,** 351–357 (1998).

29. T. Yamazaki, W. Lee, M. Revington, D. L. Mattiello, F. W. Dahlquist, C. H. Arrowsmith, and L. E. Kay, An HNCA pulse scheme for the backbone assignment of ^{15}N, ^{13}C, ^{2}H-labeled proteins: Application to a 37-kDa trp repressor-DNA complex, *J. Am. Chem. Soc.* **116,** 6464–6465 (1994).

30. I. Nesmelova, A. Krushelnitsky, D. Idiyatullin, F. Blanco, M. Ramirez-Alvarado, V. A. Daragan, L. Serrano, and K. H. Mayo, Conformational exchange on the microsecond time scale in α-helix and β-hairpin peptides measured by ^{13}C NMR transverse relaxation, *Biochemistry* **40,** 2844–2853 (2001).

31. J. W. Peng and G. Wagner, Investigation of protein motions via relaxation measurements, *Methods Enzymol.* **239,** 563–596 (1994).

32. V. Munoz, F. J. Blanco, and L. Serrano, The hydrophobic-staple motif and a role for loop-residues in α-helix stability and protein folding, *Struct. Biol.* **2,** 380–385 (1995).

33. G. M. Clore, P. C. Driscoll, P. T. Wingfield, and A. M. Gronenborn, Analysis of the backbone dynamics of interleukin-1β using two-dimensional inverse heteronuclear ^{15}N–^{1}H NMR spectroscopy, *Biochemistry* **29,** 7387–7401 (1990).

34. J. R. Lakowicz, H. Cherek, I. Gryczynski, N. Joshi, and M. L. Johnson, Enhanced resolution of fluorescence anisotropy decays by simultaneous analysis of progressively quenched samples. Applications to anisotropic rotations and to protein dynamics, *Biophys. J.* **51,** 755–768 (1987).

35. A. Tamura, M. Matsushita, A. Naito, S. Kojima, K. I. Miura, and K. Akasaka, Dynamics of the three methionyl side-chains of *Streptomyces* subtilisin inhibitor. Deuterium NMR studies in solution and in the solid state, *Protein Sci.* **5,** 127–139 (1996).